RHODIUM(0) NANOPARTICLES SUPPORTED ON HYDROXYAPATITE: PREPARATION, CHARACTERIZATION AND CATALYTIC USE IN HYDROGEN GENERATION FROM HYDROLYSIS OF HYDRAZINE BORANE AND AMMONIA BORANE

A THESIS SUBMITTED TO
THE GRADUATE SCHOOL OF NATURAL AND APPLIED SCIENCES
OF
MIDDLE EAST TECHNICAL UNIVERSITY

BY

DERYA ÇELİK

IN PARTIAL FULFILLMENT OF THE REQUIREMENTS
FOR
THE DEGREE OF MASTER OF SCIENCE
IN
CHEMISTRY

FEBRUARY 2012

Approval of the thesis:

RHODIUM(0) NANOPARTICLES SUPPORTED ON HYDROXYAPATITE: PREPARATION, CHARACTERIZATION AND CATALYTIC USE IN HYDROGEN GENERATION FROM YDROLYSIS OF HYDRAZINE BORANE AND AMMONIA BORANE

submitted by **DERYA ÇELİK** in partial fulfillment of the requirements for the degree of **Master of Science in Chemistry Department, Middle East Technical University** by,

Prof. Dr. Canan Özgen _____
Dean, Graduate School of **Natural and Applied Sciences**

Prof. Dr. İlker Özkan _____
Head of Department, **Chemistry**

Prof. Dr. Saim Özkar _____
Supervisor, **Chemistry Dept., METU**

Examining Committee Members:

Prof. Dr. Gülsün Gökağaç Arslan _____
Chemistry Dept., METU

Prof. Dr. Saim Özkar _____
Chemistry Dept., METU

Prof. Dr. Birgül Zümreoğlu Karan _____
Chemistry Dept., Hacettepe University

Assoc. Prof. Dr. Ayşen Yılmaz _____
Chemistry Dept., METU

Assist. Prof. Dr. Emren Nalbant Esentürk _____
Chemistry Dept., METU

Date: 08.02.2012

I hereby declare that all information in this document has been obtained and presented in accordance with academic rules and ethical conduct. I also declare that, as required by these rules and conduct, I have fully cited and referenced all material and results that are not original to this work.

Name, Last name: Derya Çelik

Signature

ABSTRACT

RHODIUM(0) NANOPARTICLES SUPPORTED ON HYDROXYAPATITE: PREPARATION, CHARACTERIZATION AND CATALYTIC USE IN HYDROGEN GENERATION FROM HYDROLYSIS OF HYDRAZINE BORANE AND AMMONIA BORANE

Çelik, Derya

M.Sc., Department of Chemistry

Supervisor: Prof. Dr. Saim Özkar

February 2012, 59 pages

This dissertation presents the preparation and characterization of rhodium(0) nanoparticles supported on hydroxyapatite, and investigation of their catalytic activity in hydrogen generation from the hydrolysis of hydrazine-borane and ammonia-borane. Rh^{+3} ions were impregnated on hydroxyapatite by ion-exchange; then rhodium(0) nanoparticles supported on hydroxyapatite were formed *in-situ* during the hydrolysis of hydrazine-borane at room temperature. The rhodium(0) nanoparticles supported on hydroxyapatite were isolated as black powders by centrifugation and characterized by ICP-OES, SEM, TEM, EDX, XRD, XPS, and N_2 adsorption-desorption spectroscopy. Rhodium(0) nanoparticles supported on hydroxyapatite have a mean particle size of 2.7±0.7 nm.

The catalytic activity of rhodium(0) nanoparticles supported on hydroxyapatite was tested separately in the hydrolysis of hydrazine-borane and ammonia-borane. The hydrolysis of hydrazine-borane was started by adding the precatalysts, Rh^{+3}-exchanged hydroxyapatite into the aqueous solution of hydrazine-borane; whereas, the hydrolysis of ammonia-borane was initiated by adding the catalyst rhodium(0) nanoparticles supported on hydroxyapatite which have been

isolated from the first run of hydrolysis of hydrazine-borane. Rhodium(0) nanoparticles supported on hydroxyapatite provide a turnover frequency value of 6700 h^{-1} in the hydrolysis of hydrazine-borane at room temperature. The reuse experiments reveal that these supported nanoparticles are isolable, bottlable, and redispersible in solution. Furthermore, they retain 62 % of their initial activity at the fifth run in the hydrolysis of hydrazine-borane with release of 3 equivalents hydrogen. Activity of rhodium(0) nanoparticles supported on hydroxyapatite is maintained after the redispersion of the sample and 3 equivalents hydrogen generation from the hydrolysis of ammonia-borane confirms the activity of preformed catalyst. Rhodium(0) nanoparticles supported on hydroxyapatite provide a turnover frequency value of 3990 h^{-1} in the hydrolysis of ammonia-borane at room temperature.

Keywords: Rhodium(0)nanoparticles; Hydroxyapatite; Hydrolysis; Hydrazine-borane; Ammonia-borane; Hydrogen generation.

ÖZ

HİDROKSİAPATİT ÜZERİNDE DESTEKLENDİRİLMİŞ RODYUM(0) NANOPARÇACIKLARI: HAZIRLANMASI, KARAKTERİZASYONU VE HİDRAZİN-BORAN VE AMONYAK-BORAN HİDROLİZİNDEN HİDROGEN ÜRETİMDE KATALİTİK OLARAK KULLANILMASI

Çelik, Derya

Yüksek Lisans, Kimya Bölümü

Tez Yöneticisi: Prof. Dr. Saim Özkar

Şubat 2012, 59 sayfa

Bu tez hidroksiapatit ile kararlılaştırılmış rodyum(0) nanoparçacıklarının hazırlanmasını, karakterizasyonunu, hidrazin-boran ve amonyak-boran hidrolizinden hidrojen salınımındaki katalitik aktifliğinin sınanmasını sunmaktadır. Rodyum(III) iyonları hidroksiapatit üzerinde iyon değişim ile desteklendirildi, sonra, hidroksiapatit üzerinde desteklendirilmiş rodyum(0) nanoparçacıkları oda sıcaklığında hidrazin boranın hidrolizi esnasında oluşturuldu. Hidroksiapatit üzerinde desteklendirilmiş rodyum(0) nanoparçacıkları santrifüj ile siyah toz halinde izole edildi ve ICP-OES, SEM, TEM, EDX, XRD, XPS, ve N_2 yüzey tutunma-salınma spektroskopisi methodları ile karakterize edildi. Hidroksiapatit üzerinde desteklendirilmiş rodyum(0) nanoparçacıkları 2.7 ± 0.7 nm ortalama parçacık boyutuna sahiptir.

Hazırlanan hidroksiapatit üzerinde desteklendirilmiş rodyum(0) nanoparçacıklarının katalitik aktivitesi hidrazin boranın ve amonyak boranın hidrolizinde ayrı ayrı test edildi. Rodyum(III)-değiştirilmiş hidroksiapatit katalizörü hidrazin boranın sulu çözeltisine ekleyerek hidrazin boranın hidrolizi başlatıldı, oysa, amonyak boranın hidrolizi hidrazin boranın hidrolizinden izole edilen hidroksiapatit üzerinde desteklendirilmiş rodyum(0) nanoparçacıkları eklenerek başlatıldı. Oda sıcaklığında, hidrazin boranın hidrolizinde hazırlanan katalizörün çevrim frekansı

6700 sa^{-1} tir. Tekrar kullanılabilirlik deneyleri şunu gösterir ki; desteklendirilmiş nanoparçacıklar izole edilebilir, saklanabilir ve çözeltide tekrar dağıtılabilir, ayrıca, 5. kullanımında hidrazin boranın hidrolizinde 3 eşdeğer hidrojenin salınımı ile başlangıç aktivitesinin % 62'sini korur. Hidrolizde, hidrazin boranın ilk kullanımından izole edilen madde tekrar dağıtıldıktan sonra hidroksiapatit üzerinde desteklendirilmiş rodyum(0) nanoparçacıklarının aktivitesini koruduğu ve bu aktivite 3 eşdeğer hidrojen salınımı ile amonyak boranın hidrolizi ile kanıtlanmıştır. Oda sıcaklığında, amonyak boranın hidrolizinde hazırlanan katalizörün çevrim frekansı 3990 sa^{-1} tir.

Anahtar kelimeler: Rodyum(0) nanoparçacıkları; Hidroksiapatit; Hidroliz; Hidrazin boran; Amonyak boran; Hidrojen Üretimi

To my family,

ACKNOWLEDGEMENT

I would like to express my sincere thanks to Prof. Dr. Saim Özkar for his priceless support, guidance and encouragement during my graduate studies and in the completion of this dissertation. I am deeply honored to have a chance to work with him, and to be alumni of his highly respected research group.

My appreciation and thanks to Dr. Mehmet Zahmakıran for his guidance, valuable advice, motivation, supports and positive attitude towards me during my thesis studies.

I would like to also thank to Dr. Senem Karahan for her valuable friendship, advice, and supports.

I would like to express my thanks to my labmates Melek Dinç, Tuğçe Ayvalı, Serdar Akbayrak, Ebru Ünel, Murat Rakap, Assist. Prof. Dr. Önder Metin, Assist. Prof. Dr. Sibel Duman, Selin Şencanlı and Salim Çalışkan for their friendship.

I would like to thank my roommates Cemile, Cansu, Bahar, and Chinara for their comprehension, make the dormitory life funny and priceless friendship.

I would like to thanks to TUBITAK for 2210- National Scholarship Programme for M.Sc. Students.

The last but not the least, my special appreciation and great gratitude is devoted to my dear family for their endless moral support and my fiancée Güven for his love, patience, moral support, joy and encouragement in every moment of my life.

TABLE OF CONTENTS

LIST OF FIGURES

FIGURES

LIST OF ABBREVIATIONS

ICP-OES: Inductively Coupled Plasma - Optical Emission spectroscopy

TEM: Transmission Electron Microscopy

SEM: Scanning Electron Microscopy

EDX: Energy Dispersive X-Ray

XRD: X - Ray Diffraction

XPS: X - Ray Photoelectron Spectroscopy

Uv-vis: Ultraviolet Visible Spectroscopy

NPs: Nanoparticles

NCs: Nanoclusters

HAP: Hydroxyapatite

Rh^{+3}@HAP: Rh^{+3} - Exchanged Hydroxyapatite

RhNPs@HAP: Rhodim(0) Nanoparticles Supported on Hydroxyapatite

HB: Hydrazine borane

AB: Ammonia borane

SB: Sodium borohydride

TOF: Turnover Frequency

TON: Turnover Number

E_a: Activation Energy

ICE: Internal Combustion Engine

CHAPTER 1

INTRODUCTION

The concept of using hydrogen as an energy carrier has been discussed for at least the past 30 years due to the depletion in the fossil hydrocarbon reserves [1]. Hydrogen may fulfil part of the central role currently occupied by fossil fuels and provide the mean of connection and link to a sustainable energy economy [2]. Although it is an attractive replacement for carbon-based fuels, molecular H_2 is not freely available on earth; conversely, it is bound up in chemical compounds with other elements. Therefore, energy is necessary to from elemental hydrogen; that is the reason why it cannot be referred as a primary energy source. Hydrogen, like electricity, is an energy carrier [3] and like electricity, it must be produced from natural sources.

Hydrogen economy has a network consisting of three important steps; production, storage and use. Domestic resources and renewable sources such as solar, wind, hydropower, and geothermal can be utilized in order to produce hydrogen. However, besides their relatively high cost, there is a discontinuity problem in such kind of sources. Furthermore, due to the incorporation of hydrogen with other elements, water electrolysis, photolysis, thermochemical cycles, and biomass can also be used in the production part.

Regardless of the application, hydrogen storage is a very challenging technical and economic issue to be overcome before the hydrogen economy can be realized on global scale [4]. Hydrogen can be stored physically by changing its state conditions (compressed gas or cryogenic liquid) and chemically in various solid compounds such as metal nitrides and imides [5], carbon nanotubes [6], TiO_2 nanotubes [7], zeolites [8], organic polymers [9], metal-organic frameworks [10] and carbon-boron-nitrogen (CBN) compounds [11]. Among these materials, boron-based compounds have attracted special interest due to their low weight and high

gravimetric capacity [12]. Furthermore, the results of recent studies have presented that boron-nitrogen (BN) adducts such as ammonia-borane (AB, NH_3BH_3) [13] and hydrazine-borane (HB, $N_2H_4BH_3$) [14] should be considered as promising materials for efficient hydrogen storage owing to high hydrogen content which have 19.6 and 15.4 % wt. H_2, respectively; which satisfy 2015 targets of U.S. Department of Energy (U.S. DOE) (9 % wt. H_2) [15].

AB is solid at room temperature with a low molecular weight (30.9 g/mol) and high hydrogen content (19.6 % wt.). Hydrogen can be generated from AB by dehydrogenation of both solid-state and solution approaches such as the pyrolysis of AB in solid-state [16], catalytic dehydrocoupling of AB in organic solvents [17], dehydrogenation of AB in ionic-liquid at elevated temperature [18], heating acetonitrile and etheral solution of AB for hydrogen release [19], thermal decomposition in Lewis/Brønsted acids [20], metal catalyzed thermolysis [21], base promoted dehydrogenation [22]. Another closely related BN compounds, hydrazine-borane ($N_2H_4BH_3$) is solid at the room temperature with molecular weight of 46 g/mol and 15.4 % wt. hydrogen capacity. Hydrazine-borane releases hydrogen upto 6.5 % wt. during thermolysis at 150 °C [23]. However, there is much concentration in transition metal catalyzed hydrolysis of boron-based compounds due to the favourable fast H_2 generation under mild conditions.

$$N_2H_4BH_3 + 2H_2O \xrightarrow{\text{catalyst}} N_2H_5BO_2 + 3H_2 \qquad (1)$$

$$NH_3BH_3 + 2H_2O \xrightarrow{\text{catalyst}} NH_4BO_2 + 3H_2 \qquad (2)$$

In this context, many homogeneous and heterogeneous catalysts have been employed in the catalytic hydrolysis of AB and HB [24,25]. Preference of the heterogeneous catalysis is much more than homogeneous catalysis in many applications [26] owing to their easy separation, reusability, and stability [27]. In catalytic processes, nanomaterials are of great importance and in this context, metal nanoparticles stand out owing to their high activity because of their relatively high surface-volume ratio and large number of active atoms lying on the surface [28]. The challenging issue in the application of metal nanoparticles (NPs) is the synthesis of size and shape controllable NPs because, as these are the key factors that affect the

activity and selectivity of the catalyst. Although metal NPs are not thermodynamically stable towards aggregation, they can be stabilized kinetically. As they have great tendency to aggregation, metal nanoparticles have to be stabilized against to agglomeration in order to retain their large surface area, high activity and lifetime. In this context, the stabilization of metal NPs in confined void spaces such as inside zeolites [29], carbonaceous materials [30], metal oxides [31], polymers [32], metal-organic-frameworks [33] appears as a promising way in order to inhibit further growing of NPs. In recent publications, it has been demonstrated that transition metal(0) nanoclusters confined in the cavities of zeolite-Y present outstanding catalytic activity in the hydrolysis of sodium borohydride [34] and ammonia-borane [13e,35] at the room temperature. Besides, recently, hydroxyapatite (HAP, $Ca_{10}(PO_4)_6(OH)_2$) has gained great interest as a catalyst support [36]. Recent publications have demonstrated the effective employment of HAP as support for Ru, Pd, Co in catalytic reactions of hydrogenation of aromatics, hydrolysis of ammonia borane, hydrolysis of both sodium borohydride and ammonia-borane, respectively [37]. The use of HAP as a catalyst support has been motivated by the following characteristics *(i)* high adsorption and ion-exchange ability, *(ii)* low mass transfer limitations due to low porous structure, *(iii)* reduced side reaction because of low surface acidity [38]. Both results of catalytic reactions in the presence of HAP and these important characteristics encouraged us to develop transition metal nanoparticles supported on HAP with high catalytic activity and lifetime in the hydrolysis of hydrazine-borane and ammonia-borane using the advantages of the heterogeneous catalysts [39].

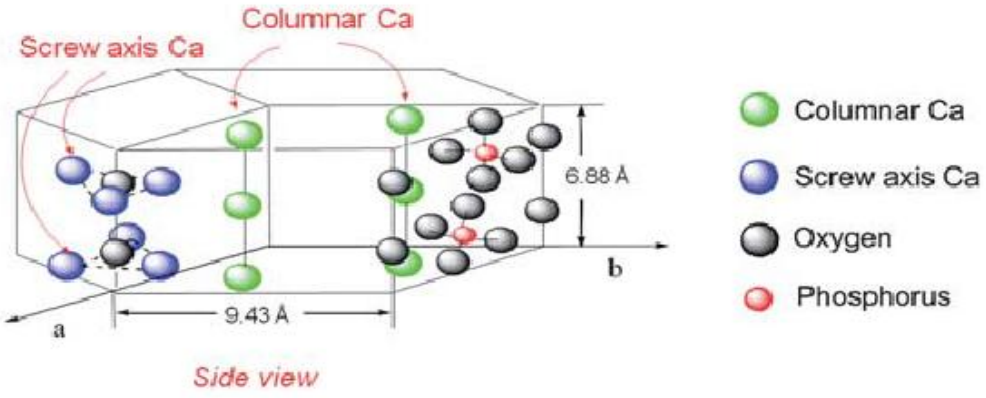

Figure 1. Structure of hydroxyapatite [38].

The aim of this study is the preparation, characterization of rhodium(0) nanoparticles supported on hydroxyapatite and their employment in the hydrogen generation from the hydrolysis of hydrazine-borane and ammonia-borane. The rhodium(0) nanoparticles stabilized on hydroxyapatite, hereafter referred to as RhNPs@HAP, were prepared by ion-exchange of Rh^{+3} ions with the Ca^{+2} cations of hydroxyapatite, then, Rh^{+3} ions were reduced *in-situ* during the hydrolysis of HB. Finally, rhodium(0) nanoparticles supported on hydroxyapatite were characterized by ICP-OES, SEM, EDX, TEM, XRD, XPS, and N_2 adsorption-desorption spectroscopy. Then, this preformed catalyst was used in the hydrolysis of AB.

RhNPs@HAP formed *in-situ* during the hydrolysis of HB show high activity in the hydrogen generation from the hydrolysis of hydrazine-borane and high performance in the reuse experiments by retaining their initial activity of 62 % even at its fifth reuse with 3 equivalents H_2 generation. In kinetic experiments, the effects of catalyst concentrations, substrate concentrations and temperature on the hydrogen generation rate were investigated.

In the next part, the preformed catalyst, RhNPs@HAP was used in the catalytic hydrolysis of AB. The activity of rhodium(0) nanoparticles supported on hydroxyapatite was maintained after the redispersion of the sample isolated from the solution after complete hydrolysis of hydrazine-borane. The evolution of 3 equivalents of hydrogen from the hydrolysis of ammonia-borane confirms the activity of preformed catalyst. Detailed kinetic experiments were performed depending on the catalyst concentrations, substrate concentrations and temperature.

CHAPTER 2

HYDROGEN

For a long time, human beings have used naturally occurring fossil fuels to produce energy. If the time order is drawn for these supplies, wood, peat, petrol and natural gas complete the list in nearly chronological order. With the Industrial Revolution in 18^{th} century, coal gained greater attention than other fuels, and then the invention of internal combustion engine was the starting point of the use of petrol as a fuel in 19^{th} century so, gradual transition from coal to oil occurred [40]. Today, the importance of petrol is still dominant as a fuel; therefore, the energy demand of world has been met 45 % from petroleum, 25 % from natural gas and 30 % from coal. Nevertheless, these fuels are carbon-based so, world faces with the depletion and shortage of the fossil fuels which means that reserves of these fuels are not sufficient for a long time to meet increasing energy demand of the world [41]. Besides, greater amount of CO_2 has been released to the atmosphere because of the burning of these fuels for a long period. Therefore, it is very crucial to introduce an alternative energy sources in order to not only prevent further growing effect of CO_2 in atmosphere, but also find a solution for the depletion of energy sources [42]. Due to the fact that, there is need a new sustainable energy transition. The concept of using hydrogen as an energy carrier has been discussed for a long time. Hydrogen as an energy carrier is a promising candidate which can be replaced by carbon-based fossil fuels to fulfil the requirements for energy demand of world and provide the mean of connection with sustainable energy economy. The main advantages of the hydrogen making it applicable can be followed;

- Many primary energy resources (sun, wind, geothermal, hydropower etc.) can be used to generate hydrogen; one of that can be reachable from anywhere in the world.
- Hydrogen is the aboundant element in the universe.

- Hydrogen is nature-friendly, non-toxic and clean; the combustion product of hydrogen with oxygen is water.
- Hydrogen can be used directly as a transportation fuel. Internal combustion engine that uses the gasoline can also work by using hydrogen directly without much different [43].
- All branches of the economy such as automobile or fuel cells can operate hydrogen.
- Hydrogen can be stored for a long time [44].

However, hydrogen cannot be found in nature as the fuel H_2. Chemical compounds such as water and hydrocarbons incorporate with hydrogen; therefore, chemical transformation is necessary for the releasing H_2. Hydrogen is an energy carrier, like electricity and can be obtained by using natural or renewable energy resources [45]. It is not only produced by different renewable sources containing wind, solar, hydro-power, geothermal, nuclear and coal, but also a number of processes; such as, thermochemical processes [46], electrochemical processes [47], photochemical processes [48]. The general recognized phenomenon for hydrogen economy is replacement of carbon-based fuels with the hydrogen which can be utilized as a fuel in internal combustion engines (ICEs), external combustion engines or fuel cells [49]. There are three basic points in hydrogen economy which are production, storage and use (Figure 2.).

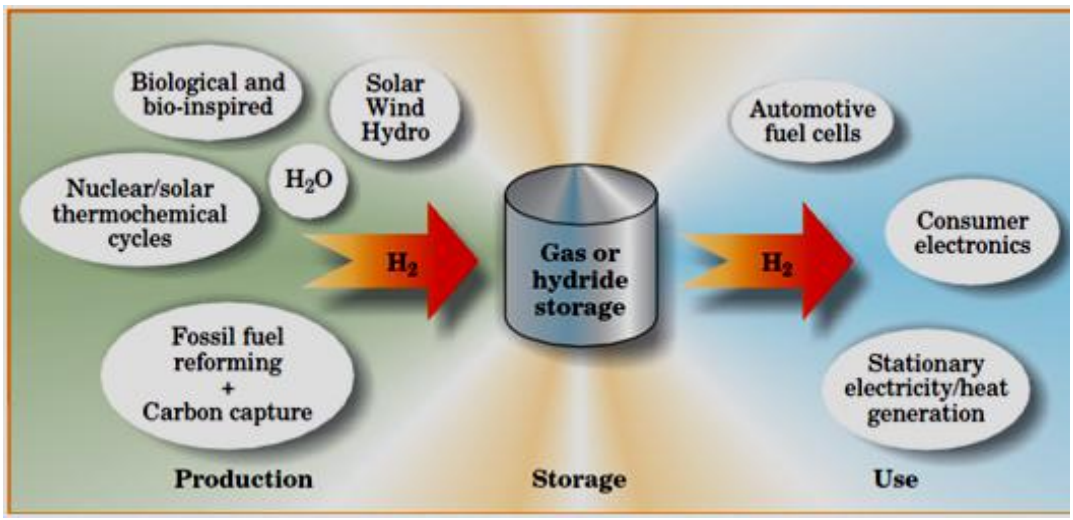

Figure 2. The hydrogen economy[45]

2.1. Hydrogen Storage

Before the acceptance of hydrogen as an alternative energy carrier, efficient hydrogen storage is a challenge issue that has to be overcome. [50]. The use of hydrogen as a transportation fuel has a main hindrance due to the relatively low energy density for on-board hydrogen applications. In fact, hydrogen has three times greater energy content than other chemical fuels, e.g. gasoline, by weight [51], whereas as volume, this value is four times less than gasoline. There are four main approaches that have been used to store and deliver the hydrogen to the use points; these are compressed gas, liquid hydrogen, metal hydrides and chemical hydrides. Compressed gas form and liquid hydrogen can be thought as only near term solution because these approaches are limited due to the low volumetric energy density and cryogenic requirements. For long term, many researchers have studied to get better storage alternatives and in this context, chemical approaches have gained great attention, in which there is a chemical bonding between hydrogen and other elements [52]. The important requirements for hydrogen storage system are the minimum weight and volume; however, high energy supply. Furthermore, the 2015 target of the U.S. Department of Energy is 9 % wt. hydrogen for materials to be practically applicable [15]

Various studies have been performed [40] for many years so as to find better options for the storage of the hydrogen. Among these studies, owing to the high gravimetric/volumetric hydrogen storage ability [53] and high energy density for H_2 storage, complex hydrides are found as most convenient systems. In the complex hydrides, boron-based compounds have gained much concern due to their high hydrogen capacity, low molecular weight, solubility (Figure 3) [54].

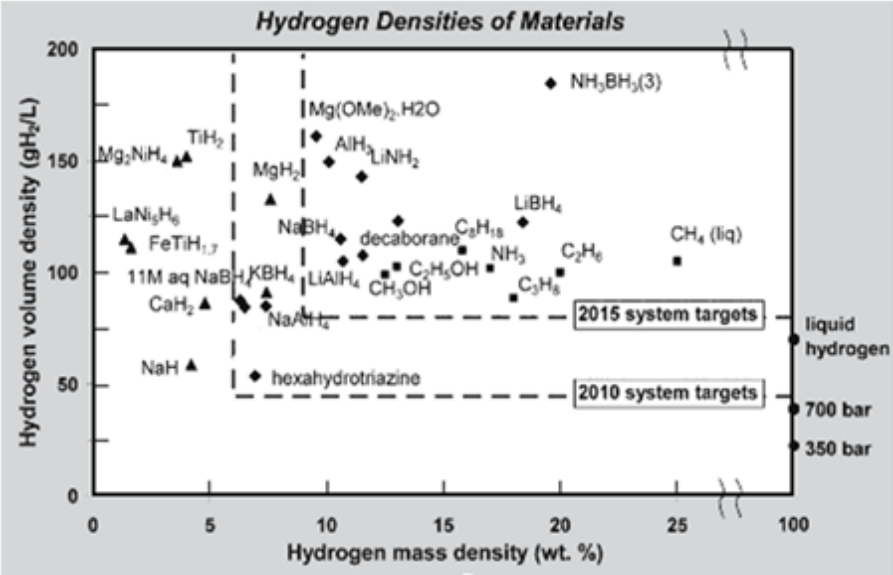

Figure 3. Hydrogen mass density vs hydrogen volume density for many hydrogen storage materials [54].

Discovery of sodium borohydride (SB) extended to 1940s [55] however there was no effective use of SB in the means of energy context until the late of 1990s. The rising demand towards renewable energy sources and energy carrier was reminded SB as a hydrogen storage compounds [56] and as a fuel for direct proton exchange membrane fuel cells [57] and after that, many researchers spent great afford and published many papers that was the indication of the rising interest toward SB [58]. However, U.S. Department of Energy published a report about no longer use of SB as hydrogen storage material on-board vehicle because the targets of U.S. DOE about storage capacity, spent fuel recycling and cost are not met by the aqueous solution of SB [59]. On the other hand, this report makes positive contribution to the use of ammonia-borane for on-board hydrogen storage.

Ammonia-borane with low molecular weight (30.9 g mol^{-1}) and high hydrogen capacity (19.6 % wt) is the simplest B-N compound and has a great attention as a promising boron-based compound for on-board hydrogen storage applications in recent years [60]. In ammonia-borane, B-N bond is a dative bond formed by the interaction of the nonbonding electron pair of NH_3 and empty P_z orbital of boron in BH_3 [61] as an electron donor–acceptor complex. In ammonia-

borane, hydrogens on nitrogen are protonic and hydrogens on boron are hydridic due to the distinct electronegativities of nitrogen and boron which are 3.04 and 2.04, respectively. (Figure 4).

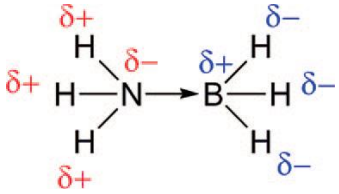

Figure 4. N-H and B-H bond polarizations in ammonia borane [62].

Ammonia-borane has staggered conformation with B-N bond length of 1.564 Å (6), B-H bond length of 0.96 (3)-1.18 (3) Å and N-H bond length of 0.96-1.14 (2) Å [63]. Hydrogen can be liberated from AB by dehydrogenation of both solid-state and solution approaches. Besides, the catalytic hydrolysis of AB supplies a more promising way for hydrogen production in high purity and very controllable rates, thus; 3 equivalent gases can be released in the presence of suitable catalysts.

$$NH_3BH_3 + 2H_2O \xrightarrow{\text{catalyst}} NH_4BO_2 + 3H_2 \qquad (3)$$

The other derivative of B-N compounds is the hydrazine-borane which should also be considered as a hydrogen storage materials because of the hydrogen storage capacity of 15.4 % wt. ($4H^+$, $3H^-$) that satisfy 2015 targets of the U.S. DOE. This closely related compound can be produced from the reaction of dihydrazine sulfate and sodium borohydride in cyclic ethers and its melting point is 61 °C. After that temperature, slow decomposition of compound starts. Thermolytically hydrogen release of hydrazine-borane exhibits that hydrogen release occurs slowly and 6.5 % wt. is given off upon heating upon to 150 °C in 16 h [64]. Nevertheless, catalytic hydrolysis of hydrazine-borane in the presence of appropriate catalyst also causes the fast release of 3 equivalent H_2 gas with controllable rates [65].

$$N_2H_4BH_3 + 2H_2O \xrightarrow{\text{catalyst}} N_2H_5BO_2 + 3H_2 \qquad (4)$$

In this dissertation, hydrogen generation from the hydrolysis of hydrazine-borane and ammonia-borane catalyzed by rhodium(0) nanoparticles supported on hydroxyapatite were investigated. In this context, the effects of catalyst concentration, substrate concentrations and temperature on the reaction rate were studied to highlight the kinetic of the reactions and find activation parameters of the reactions.

CHAPTER 3

TRANSITION METAL(0) NANOCLUSTERS

3.1.General Introduction

The term nanoclusters (NCs) can be used to define a matter whose size is larger than typical molecules; however, the size of which is so small to represent properties of bulk materials [66]. Metal nanoclusters should have the following criteria (a) less than 15 % size dispersion with smaller particle size than 10 nm (b) well defined composition (c) reproducible syntheses (control over size, shape and composition) (d) isolability, bottlability, and redissolvability [67,68].

Due to the size range and properties of metal NCs, they are subject of many researches [69]. The great and increasing interest toward these materials is derived from not only getting information about their novel chemical, physical and size–dependent phenomena on the nanometer length scale but also developments and beneficial uses of them in many applications containing, quantum dots [70], quantum computers [71] and devices [72], chemical sensors [73], light-emitting diodes [74], flat panel displays [75], highly active and selective catalysts [76].

Metal NCs demonstrate unique and interesting physical and chemical properties. This can be observed in Figure 5 showing that the large numbers of the metal atoms lie on the surface, which means that the decrease in particle size causes the increasing in the number of the atoms on surface. Besides, the surface atoms do not necessarily order themselves in the same way that those in the bulk do [77].

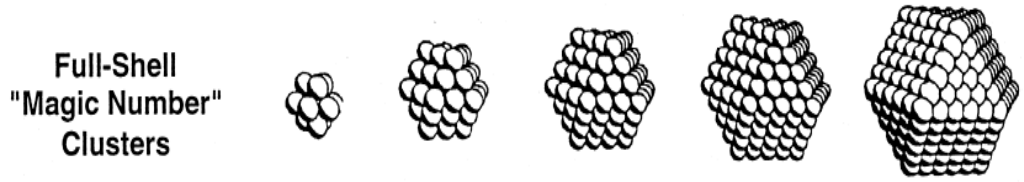

Number of shells	1	2	3	4	5
Number of atoms in cluster	M_{13}	M_{55}	M_{147}	M_{309}	M_{561}
Percentage surface atoms	92%	76%	63%	52%	45%

Figure 5. The relation between the total number of atoms in full shell clusters and the percentage of surface atoms [78].

With respect to electronic structures, clusters are intermediate between mononuclear coordination compounds and bulk metals. The presence of energy bands is characteristic for electronic situation in bulk metals. A great number of energetically similar orbitals come together to form energy band. There is an overlap between valence band and conduction band of metals. The reduction of size in metal particles causes the disappearance of the coalescence between valence and conduction band, thus further reduction in particle size leads to turn from bands to more or discrete energy levels. At this step, the bulk properties of material start to disappear and also electronic properties alter dramatically [79].

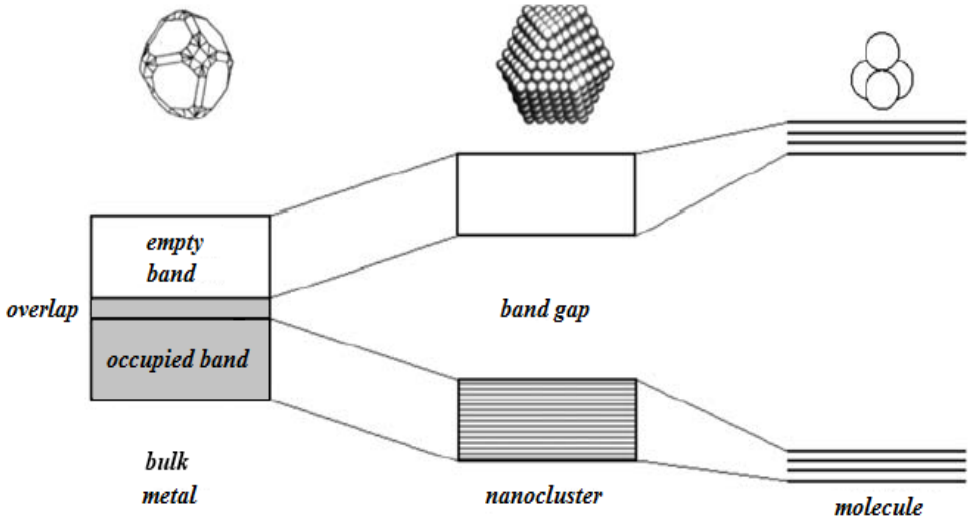

Figure 6. Schematic illustration of electronic levels in bulk metal, nanocluster and molecule, respectively [79].

3.2. Stabilization of Transition Metal Nanoclusters

The lifetime of clusters or colloids is short in solution after the syntheses from their corresponding metal salt or a complex in an appropriate solvent because clusters and colloids have a tendency for further aggregation and form their larger arrangements due to their thermodynamic instability. However, one of the most important properties of colloidal particles is the small size in which they have kinetic stability. The main power for aggregation is the van der Waals forces between two metallic particles that cause the attraction to each other at short distances; therefore, the presences of repulsive forces are necessary so as to inhibit further growing. Derjagin-Landau-Verwey-Overbeek (DLVO) [80] developed in 1940's is a theory describing the general stabilization mechanisms of colloidal materials. The general approaches in the stabilization of metal NCs are; *(i)* electrostatic stabilization, *(ii)* steric stabilization *(iii)* electrosteric stabilization.

3.2.1. Electrostatic Stabilization

The existence of ionic compounds in solution (e.g. Cl^-, $citrate^{-3}$, others) is the reason of electrostatic stabilization. The ions and also their corresponding counterions in medium are adsorbed on electrophilic metal surface [81]; thus, generation of electrically double layers around particles [82] cause the formation of Coulombic repulsion, opposing van der Waals force, between metallic particles (Figure 7). If the electric potential associated with the double layer is high enough, electrostatic repulsion will prevent particle agglomeration [67].

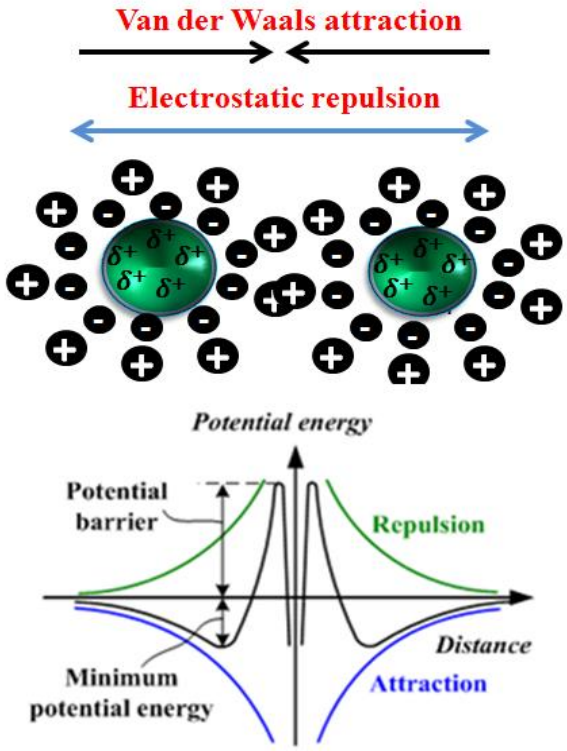

Figure 7. Electrostatic stabilization for transition metal nanoclusters and plot of energy *versus* distance between colloids [83].

3.2.2. Steric Stabilization

In this form of stabilization, aggregation of the metallic colloids can be inhibited by polymers or oligomers. Steric repulsion keeps colloidal dispersions intact which means that there is no agglomeration. Materials used in this process contain polymers or surfactants. Polymers can bind tightly to metal NPs via chemical bonding or form loosely adsorbed assemblies by physisorption mechanisms. The formation of a diffusion barrier due to the attachment of polymeric groups is the main emphasis of this type of stabilization. Consequently, metal NPs with monodisperse size can be synthesized [84].

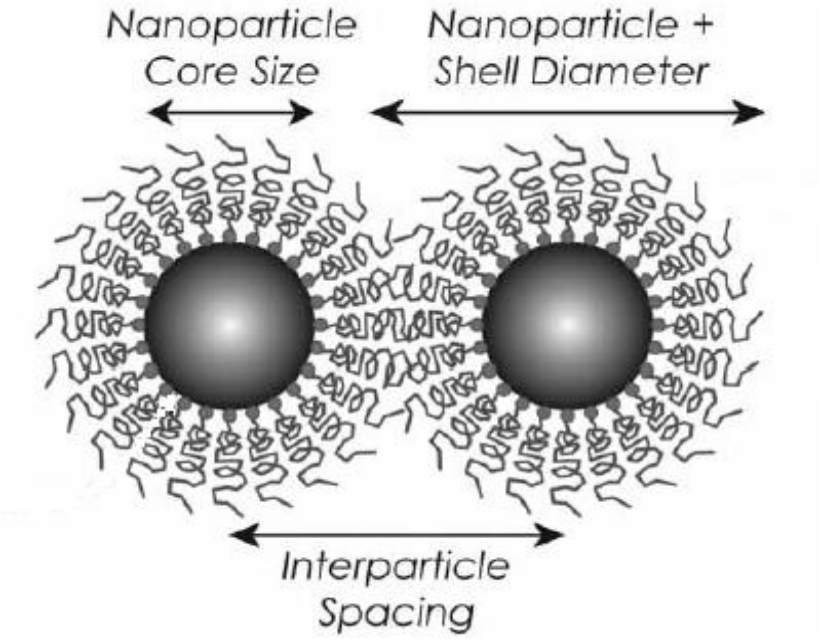

Figure 8. Schematic image of steric stabilization by adsorption of polymer chains onto a nanoparticle [85].

3.2.3. Electrosteric Stabilization

In order to make metal nanoparticles thermodynamically stable in solution, the combination of electrostatic and steric stabilization can also be used. The main characteristic is the adsorption of bulky groups such as polymers and surfactants at the surface of particles. These sterically surface active protecting layers coordinate

strongly to the metal particle's surface and, at the same time, are very well solvated in the respective medium [79].

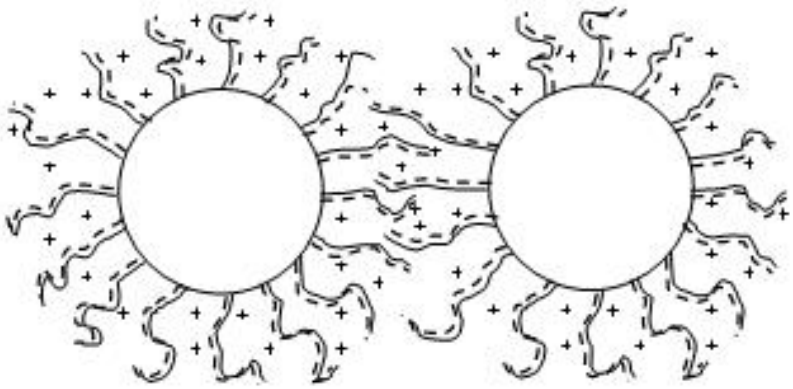

Figure 9. Schematic illustration of electrosteric stabilization of transition metal nanoparticles.

3.3. Fabrication of Metal Nanoparticles

In modern applications, the aim in the synthesis of transition metal nanoparticles is finding reproducible metal NPs syntheses protocols in order to obtain not only specific size between 1-10 nm, but also well defined surface composition of metal NPs having isolable and redissolvable properties [67]. Transition metal NCs can be fabricated by two main strategies: *top down* and *bottom up* approaches. The starting point of top down approaches is the bulk materials (top) which are broken down to metal NPs by the way of physical, chemical, thermal or mechanical processes; on the other hand, bottom up approaches start with atoms or molecules (bottom) which react under chemical or physical circumstances to generate metal NPs. Growth proceeds in zero, one or two dimensions to form dots, wires or thin films, respectively [86]. The metal NPs obtained at the end of top down processes have very broad particle size distribution (>10 nm) which means that it is very difficult to get monodispersed particles and they are not reproducibly prepared giving irreproducible catalytic activity [87]; whereas, synthesis of monodispersed particles is the main intention of the bottom up approach. In this context, the most convenient ways to control the size of metal NPs are the chemical methods, in other words, bottom up methods. The different chemical approaches are performed to prepare transition metal NPs and these methods are; *(i)* chemical reduction of transition metal complexes [88], *(ii)*

thermal or photochemical decomposition [89], *(iii)* decomposition of organometallics [90], *(iv)* metal vapor synthesis [91], *(v)* electrochemical reduction [92] *(vi)* atomic layer deposition [93], *(vii)* precipitation from reverse micelle emulsions [94] *(viii)* sol-gel technique [95].

3.4. Catalytic Applications of Transition Metal Nanoparticles

3.4.1. Catalysis

In modern world, economic and social structures are affected enormously by the use of catalysts. By the year of 2010, a great amount of catalysts have been utilized each year to produce valuable goods [96]. Catalysts have been used many different industrial areas to produce fertilizers, fuels, chemicals, medicines, textiles etc. Furthermore, catalysts also have an important impact on the quality of life from environmental perspective; for instance, the emission level of toxic gases from automobiles can be controlled by catalysts consisting rhodium, palladium, platinum and other compounds. In this context, the question that is "What is catalyst?" should be identified.

Jöns Jacob Berzelius is a Swedish chemist who firstly introduced the use of the term "catalyst" in his research about catalytic decomposition of hydrogen peroxide that was pressed in Edinburg Philosophical Journal in 1836. Berzelius evaluated and correlated the observations of earlier chemists and utilized small amounts of a catalytic substance that enhances the rate of the reaction by giving a special power. This substance is obtained at the end of the reaction without being deformed and consumed itself. The valid definition of catalyst that is used in modern world was made by Ostwald in 1894, thus; a catalyst is a substance that enhances the rate of the reaction but emerges from the process unchanged. In catalytic reaction, a new molecular mechanism is offered with the alteration of the reaction rate.

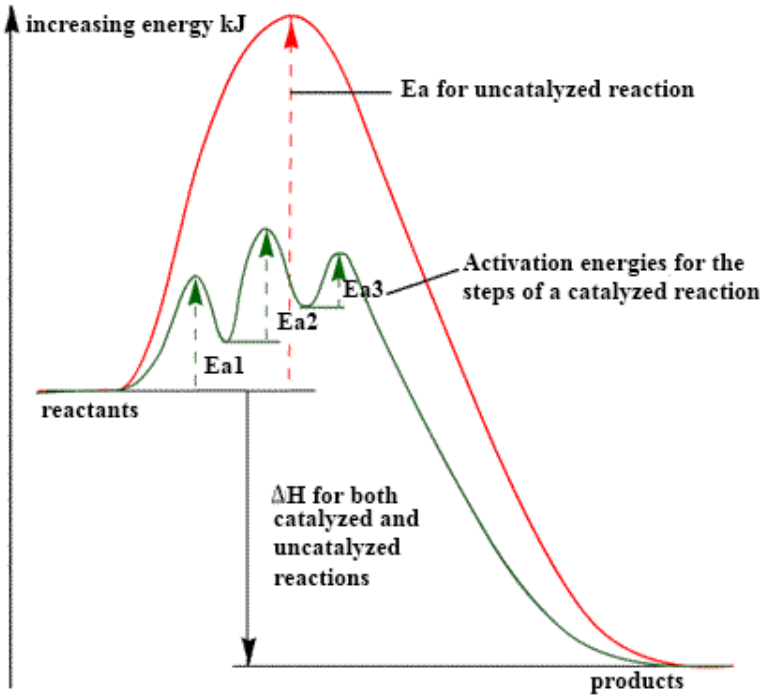

Figure 10. Different reaction paths for catalyzed and uncatalyzed reactions [97].

In addition to different reaction pathway, the use of the catalyst also has an influence on the selectivity of the reaction; therefore, more desired products can be manufactured that is the mean of increasing yield of reaction. In catalytic processes, three main characteristics of the catalyst are very crucial in order to get better results and these are activity, selectivity and stability (tendency of deactivation). The activity of the catalyst in a reaction can be evaluated by turnover number. The *total turnover number* defines the maximum utilization of a catalyst in a specified reaction under definite circumstances by a number of reactions or reaction cycles occurring at the reactive center until the decay of activity.

$$\mathrm{TTON} = \frac{\text{mol of product}}{\text{mol of catalyst}} \qquad (5)$$

The other parameter *turnover frequency* (TOF) used to specify the activity of catalyst is related to turnover number. For the reaction between A and B that is catalyzed by Q and with the rate ν, Eq. 2; and TOF is calculated from Eq. 3, where the Q is the mole of catalyst.

$$A \xrightarrow{catalyst} B$$

$$v = \frac{d[\mathrm{B}]}{d\mathrm{t}} \qquad (6)$$

$$\mathrm{TOF} = \frac{v}{\mathrm{catalyst}} \qquad (7)$$

The second important parameter for catalytic process is the selectivity of the catalyst that is the ratio of the amount of starting material to desired product. In industrial applications, the selectivity is of great importance so as to get desired products. Syn-gas reaction is one of the example in which different catalysts cause the formation of distinct products [98].

The last important characteristic of the catalysts is the stability because the chemical, thermal or mechanical stability detect the lifetime of catalyst in reaction. The stability of the catalysts can be numerously affected from the decomposition or poisoning effects which are the deactivation reasons during reaction time. The catalyst stability and lifetime are of important for the economics of the process.

3.4.2. Classification of Catalysts

There are 3 main categorizes in the classification of catalysts and these are homogeneous, heterogeneous and biocatalysts.

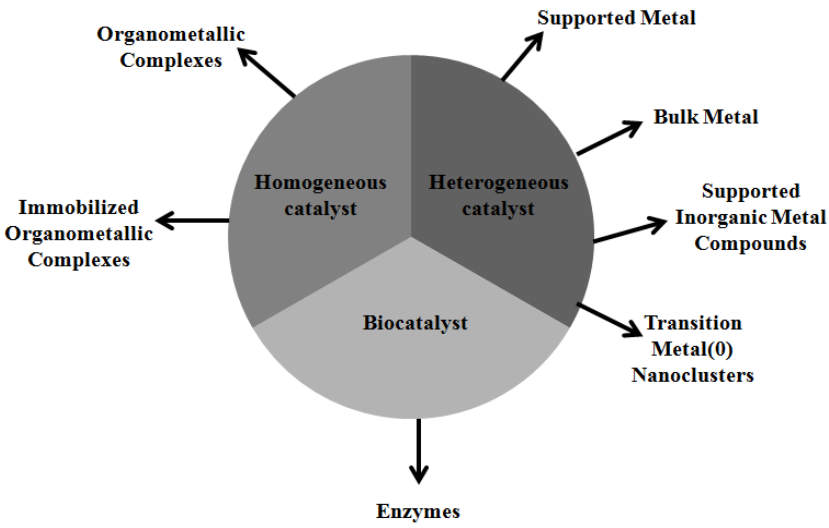

Figure 11. Classification of catalysts [99].

In homogeneous catalysis, catalytic processes occur in a uniform phase, it means that catalyst is in the same phase with reactants and products. They are generally well-defined chemical compounds or coordination complexes that are molecularly dispersed in the reaction medium [100]. On the other hand, there are more than one phases in the process of heterogeneous catalyst; besides, catalyst is generally in the solid form while reactants can be liquids or gases. In many applications, preference of the heterogeneous catalyst is much more than homogeneous catalyst due to their easy and complete separation from reaction solution. The simple separation properties of this kind of catalyst provide the reuse of quite valuable compounds. The final type of catalyst being a rather special case between homogeneous and heterogeneous catalysts is biocatalyst that is an enzyme in most cases. Biocatalysts, enzymes, present high catalytic activity in living cells; for instance, 1000 catalytic cycles can be run in one second [99a].

3.4.3. Characterization of Transition Metal Nanoparticles

Due to the growing interest to nanoparticles and the achievement in the synthesis of these valuable particles, there is a need also completely understand the composition and environment of metal NPs. Therefore, in recent years, the detailed structural and surface analyses of the catalysts have been investigated by the

chemists and physico-chemists. Today, there are a number of techniques in order to establish particle size and overall composition. One of the most widely used techniques is transmission electron microscopy (TEM) from which information about size, shape, structure, dispersion and morphology of metal nanoparticles [101] can be obtained; moreover, the utilization of high resolution instruments to examine the crystal structures and lattice spacings of metal nanoparticles is also rising and this is the high resolution transmission electron microscopy (HR-TEM). Powder X-Ray diffraction (XRD) is another method to analyze the structure of metal NPs whether they are crystalline or amorphous in nature, as well as crystallite size, crystallographic, compositional and chemical inhomogeneties are obtained from XRD. In addition, X-Ray photoelectron spectroscopy (XPS) can be used to investigate elements and their distribution on surface of metal NPs stabilized on a support or present in powder form; besides, chemical and electronic state are investigated. The other common techniques in characterization period is the UV-visible spectroscopy (Uv-vis) that is very effective to analyze semiconductor or metal NPs whose plasmon resonance is in the visible range [86]. The shape and size are the important parameters that affect the wavelengths of the metal NPs; therefore, the information about shape, size, surface composition and environment of metal NPs can also be obtained by UV-vis. Additionally, the reduction of metal precursors and the formation of the metal NPs in the presence of a stabilizer can be followed nicely [102]. As well as all of them, energy dispersive X-ray spectroscopy (EDX), scanning electron microscopy (SEM), scanning tunnelling microscopy (STM), infrared spectroscopy (ATR-IR, FTIR), atomic force microscopy (AFM), elemental analysis (ICP-OES) are the common techniques used in the characterization of the metal NPs.

CHAPTER 4

EXPERIMENTAL

4.1.Materials

Rhodium chloride trihydrate ($RhCl_3.3H_2O$), hydroxyapatite ($Ca_{10}(OH)_2(PO_4)_6$), sodium borohydride ($NaBH_4$), ammonia-borane (NH_3BH_3), and tetrahydrofuran (THF) were purchased from Sigma-Aldrich. Dihydrazine sulphate ($N_2H_4 \cdot 0.5H_2SO_4$) (98%) was purchased from Acros-Organics. Tetrahydrofuran was distilled over sodium/benzophenone under argon and stored in the drybox (H_2O and O_2 < 1 ppm). All glassware and Teflon coated stirrer bars were washed with acetone, followed by copious rinsing with distilled water before drying in oven at 150 ˚C.

4.2. Characterization

The rhodium content of Rh^{3+}-exchanged HAP was determined by ICP-OES (Inductively Coupled Plasma Optical Emission Spectroscopy). The XPS analysis was performed on a Physical Electronics 5800 spectrometer equipped with a hemispherical analyzer and using monochromatic Al Kα radiation (1486.6 eV, the X-ray tube working at 15 kV, 350W and pass energy of 23.5 keV). The X-ray diffraction (XRD) pattern was recorded on a MAC Science MXP 3TZ diffractometer using Cu-Kα radiation (wavelength 1.5406Å, 40 kV, 55 mA).

Transmission electron microscopy (TEM) was performed on a JEM-2010F microscope (JEOL) operating at 200 kV. A small amount of powder sample was placed on the copper TEM grid. Samples were examined at magnification between 100 and 400 K. Scanning electron microscope (SEM) images were taken using a JEOL JSM- 5310LV at 15 kV and 33 Pa in a low-vacuum mode without metal coating on aluminium support. The elemental analysis was performed by using an energy dispersive X-ray (EDX) analyzer (KEVEX Delta series) mounted on the Hitachi S-800.

The nitrogen adsorption/desorption experiments were carried out at 77 K using a NOVA 3000 series Quantachrome Instrument. The sample was out gassed under vacuum at 573 K for 3 h before the adsorption of nitrogen. The solution NMR studies were carried out by using Avance DPX 400 MHz spectrometer (400.1 MHz for ^{1}H NMR; 100.6 MHz and 128.2 MHz for ^{11}B NMR). $Si(CH_3)_4$ and $BF_3.(C_2H_5)_2O$ were used as internal references for ^{1}H and ^{11}B NMR chemical shifts, respectively.

4.3. Synthesis and Characterization of Hydrazine-Borane ($N_2H_4BH_3$)

Hydrazine-borane ($N_2H_4BH_3$) was prepared by the reaction of dihydrazine sulfate with sodium borohydride in cyclic ethers such as tetrahydrofuran and identified according to literature procedure [103]. The melting point of hydrazine-borane: ~ 60 °C; (DP-MS) m/z = 46 (45.87 calculated for $N_2H_4BH_3$); ^{1}H NMR (400.1 MHz, CD_2Cl_2) 5.1 ppm (t, 2, NH_2-NH_2-BH_3), 3.4 ppm (b, 2, H_2N-NH_2-BH_3), 1.2 ppm (t, 3, H_2N-NH_2-BH_3); ^{11}B NMR (128.2 MHz, H_2O) -20 ppm (q, BH_3); ATR-IR (selected, cm^{-1}) 3310 (s), 3200 (s), 2840 (m), 2650 (m), 2370 (m), 2214 (m), 1620 (s), 1588 (m), 1435 (w), 1332 (m), 1150 (s), 910 (m), 747 (w) in agreement with the literature values [104].

4.4. Preparation of Rh^{+3}-Exchanged Hydroxyapatite

Rh^{+3} cations were impregnated onto hydroxyapatite by ion exchange [104] of 1000 mg calcium(II)-exchanged hydroxyapatite in 100 mL aqueous solution of $RhCl_3.3H_2O$ (222 mg, 0.86 mmol) for 72 h at room temperature. Then, the resulting solution was centrifuged at 10000 rpm for 10 min and solid part was separated from solution and washed three times with 20 mL of deionized water and dried under vacuum (10^{-3} Torr) at 80 ˚C.

4.5. General Procedure for *in-situ* Generation of Rhodium(0) Nanoparticles Supported on Hydroxyapatite (RhNPs@HAP) During the Hydrolysis of Hydrazine-Borane and Hydrogen Generation Data Handling

The *in situ* formation of RhNPs@HAP and the concomitant hydrolysis of hydrazine-borane were performed in a jacketed reaction flask. In order to measure

hydrogen liberated during hydrolysis reaction, an experimental set-up was designed. A jacketed reaction flask with a stir bar was placed on magnetic stirrer and reaction flask was connected to water circulator to keep temperature at 25.0 ± 0.1 ˚C. Jacketed reaction flask was attributed to a graduated glass tube filled with water in order to determine hydrogen gas evolving from hydrolysis reaction. (Figure 12) In one set of experiment, firstly desired amount of Rh^{3+}@HAP was dispersed in 7.0 mL water and then this solution was transferred into jacketed reaction flask thermostated 25.0 ± 0.1 ˚C. In another flask, 46.0 mg (1 mmol) $N_2H_4BH_3$ or 31.8 mg (1mmol) NH_3BH_3

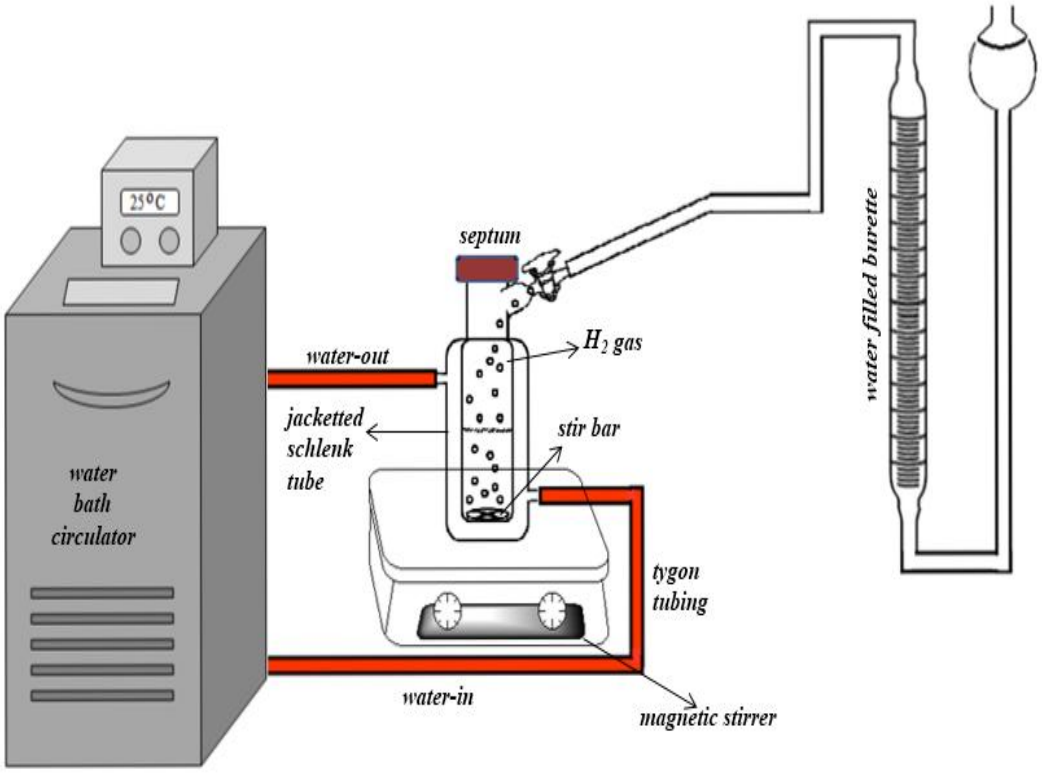

Figure 12. Experimental set-up used for determining hydrogen gas generation during reactions and also to study kinetic experiments.

(corresponding to maximum amount of H_2 gas of 3 mmol = 80.7 mL at 25.0 ± 0.1 ˚C and 0.91 atm pressure) was dissolved in 3.0 mL water and then was injected to solution containing catalyst. The experiment was started by closing the jacketed flask

with a septum and switching on magnetic stirring at 1000 rpm simultaneously. When no more hydrogen generation was observed the experiment was stopped, disconnected from the line, and the hydrogen pressure was released. In addition to volumetric measurement, the progress of the reaction was monitored by comparing the intensities of signals of hydrazine-borane and borate anion at δ= -20 (q) and 12.5 ppm (s), respectively, in the ^{11}B NMR spectra of the solution.

4.6. Kinetic Studies for RhNPs@HAP Catalyzed Hydrolysis of Hydrazine-Borane

In order to establish the rate law of RhNPs@HAP catalyzed hydrolysis of hydrazine-borane, two different sets of experiment were performed. In the first set of experiments the concentration of rhodium was kept constant at 0.5 mM (52 mg Rh^{3+}@HAP in 10 mL) and $N_2H_4BH_3$ concentration was altered in the range of 50, 100, 150, 200, 400, 600 and 800 mM (23, 46, 69, 92, 184, 276 and 368 mg $N_2H_4BH_3$ respectively). In the second set, the hydrazine-borane concentration was kept constant at [$N_2H_4BH_3$] = 100 mM (46mg $N_2H_4BH_3$) and rhodium concentration was changed in the range of 0.05, 0.10, 0.20, 0.40 and 0.60 mM (5.2, 10.4, 20.8, 41.6 and 62.4 mg Rh^{3+}@HAP, respectively).

4.7. Determination of Activation Parameters for RhNPs@HAP Catalyzed Hydrolysis of Hydrazine-Borane

In order to determine activation parameters (E_a, $\Delta H^{\#}$, and $\Delta S^{\#}$) for the RhNPs@HAP catalyzed hydrolysis of hydrazine-borane a series of experiments was performed in which hydrolysis of 100 mM $N_2H_4BH_3$ was catalyzed by RhNPs@HAP [Rh = 0.25 mM] at different temperatures (20, 25, 30, 35 and 40 °C). The values of observed rate constants k_{obs} for catalytic hydrolysis of $N_2H_4BH_3$ were determined for each temperature and utilized to calculate the activation energy by using Arrhenius plot; enthalpy and entropy of activation by using Eyring- Polanyi plot.

4.8. Catalytic Lifetime and Reusability of RhNPs@HAP in the Hydrolysis of Hydrazine-Borane

Catalytic lifetime experiment was initiated by adding 43 μmol rhodium and 4 mmol hydrazine borane at 25.0 ± 0.1 ˚C. When the expected amount of hydrogen was generated, a new batch hydrazine borane was added into solution and same procedure was applied until no more hydrogen generation was observed.

In the reusability experiments, after the first run of catalytic hydrolysis of 100 mM $N_2H_4BH_3$ (46 mg $N_2H_4BH_3$ in 10 mL) with RhNPs@HAP (50 mg) at 25.0 ± 0.1 ˚C, the catalyst was isolated from reaction solution by centrifugation and washed with excess water, then dried under vacuum. The dried catalyst was weighted and used again in the hydrolysis of 100 mM $N_2H_4BH_3$ at 25.0 ± 0.1 ˚C. The same procedure was applied throughout 4 more experiments and results were expressed as percentage initial catalytic activity of RhNPs@HAP in the hydrolysis of hydrazine-borane.

4.9. Kinetic Studies for RhNPs@HAP Catalyzed Hydrolysis of Ammonia-Borane

In this part of the experiment, the rate law for catalytic hydrolysis of NH_3BH_3 was determined. First of all, RhNPs@HAP was formed from the catalytic hydrolysis of $N_2H_4BH_3$. For this reason, solid part was seperated from reaction medium by centrifugation and washed three times with 20 mL water to remove residue, then dried under vacuum (10^{-3} Torr) at 80^0C; transferred into the drybox. In order to establish the rate law, firstly concentration of rhodium was kept constant at 0.5 mM (53.6 mg RhNPs@HAP in 10 mL) and NH_3BH_3 concentration was varied in the range of 50, 100, 150, 200 and 300 mM (15.9, 31.8, 47.7, 63.6 and 95.5 mg NH_3BH_3, respectively). In the second set, while NH_3BH_3 concentration was constant at 100 mM (31.8 mg NH_3BH_3), rhodium concentration was altered in the range of 0.05, 0.10, 0.20, 0.40 and 0.80 mM (5.4, 10.7, 21.4, 42.9 and 85.8 mg RhNPs@HAP, respectively).

4.10. Determination of Activation Parameters for RhNPs@HAP Catalyzed Hydrolysis of Ammonia-Borane

In order to determine activation parameters (E_a, $\Delta H^{\#}$, and $\Delta S^{\#}$) for the RhNPs@HAP catalyzed hydrolysis of ammonia-borane, same procedure mentioned in 4.6 was applied; therefore, a series of experiments was performed in which hydrolysis of 100 mM NH_3BH_3 was catalyzed by RhNPs@HAP [Rh = 0.25mM] at different temperatures (20, 25, 30, 35 and 40 °C). The values of observed rate constants k_{obs} for catalytic hydrolysis of NH_3BH_3 were determined for each temperature and used to calculate the activation energy by using Arrhenius plot; enthalpy and entropy of activation by using Eyring- Polanyi plot.

4.11. Catalytic Lifetime of Rhodium(0) Nanoparticles Supported on Hydroxyapatite in the Hydrolysis of Ammonia-Borane

Catalytic lifetime experiment of ammonia-borane was started by adding 46 μmol Rh and 1 mmol ammonia borane into the reaction flask at 25.0 ± 0.1 °C. When the complete hydrogen generation was observed for 1mmol AB, more substrate was added to reaction medium until no more hydrogen generation was observed indicating deactivation of the catalyst.

CHAPTER 5

RESULTS AND DISCUSSIONS

5.1. Preparation and Characterization of Rhodium (0) Nanoparticles Supported on Hydroxyapatite

The initial step of this dissertation was the preparation of Rh^{+3}-exchanged hydroxyapatite. For this purpose, Rh^{+3} ions were impregnated on the HAP by ion-exchange [104]. Then, Rh^{+3} ions on hydroxyapatite was reduced to rhodium(0) nanoparticles *in-situ* during the hydrolysis of hydrazine-borane. The change in the color of the suspension indicates the occurrence of reduction. Before the reduction, the color of supported catalyst in the powder form was pale orange. After reduction, the immediate change from orange to black was observed within a few second. This is an indication of the reduction of Rh^{+3} ions to rhodium(0) nanoparticles.

The *in-situ* formed rhodium(0) nanoparticles supported on hydroxyapatite were isolated from the reaction solution after hydrolysis reaction of hydrazine-borane by centrifugation at 10000 rpm for 10 min and stored under inert gas atmosphere. The RhNPs@HAP were characterized by ICP-OES, SEM, TEM, EDX, XRD, XPS, and N_2 adsorption-desorption spectroscopy. Figure 13 shows powder X-ray diffraction (XRD) patterns of hydroxyapatite, rhodium(III)-exchanged hydroxyapatite (Rh^{3+}@HAP) and rhodium nanoparticles supported on hydroxyapatite (RhNPs@HAP). The comparison of three XRD patterns indicates that there is no detectable alteration neither in intensities nor in positions of the main Bragg peaks observed for the hydroxyapatite matrix. Based on this observation, one can conclude that the procedure followed in the preparation of RhNPs@HAP does not cause any alteration in the framework lattice and crystallinity of the host material hydroxyapatite.

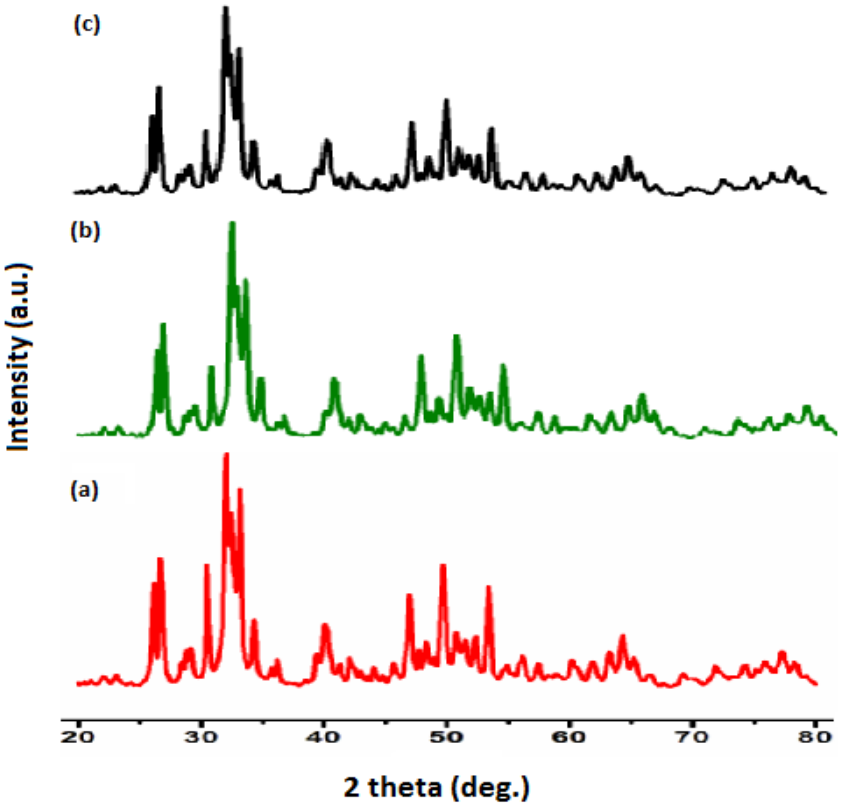

Figure 13. Powder X-ray diffraction (PXRD) patterns of (a) hydroxyapatite ($[Ca_5(OH)(PO_4)_3]_x$), (b) Rh^{+3}-exchanged hydroxyapatite (Rh^{3+}@HAP) and (c) rhodium(0) nanoparticles supported on hydroxyapatite (RhNPs@HAP).

Furthermore, the elemental analysis by inductively coupled plasma optical emission spectroscopy (ICP-OES) exhibits a rhodium loading of 0.99 % wt. for the sample. The other morphological and compositional analyses also were done in order to demonstrate the presence and the formation of RhNPs@HAP.

The next technique was scanning electron microscopy (SEM) giving information about surface of the prepared catalyst. Figure 14 depicts the SEM images of RhNPs@HAP with a rhodium loading of 0.99 % wt. in different magnifications. The inspection of these SEM images clearly shows that no bulk rhodium metal is formed in detectable size on the surface of hydroxyapatite.

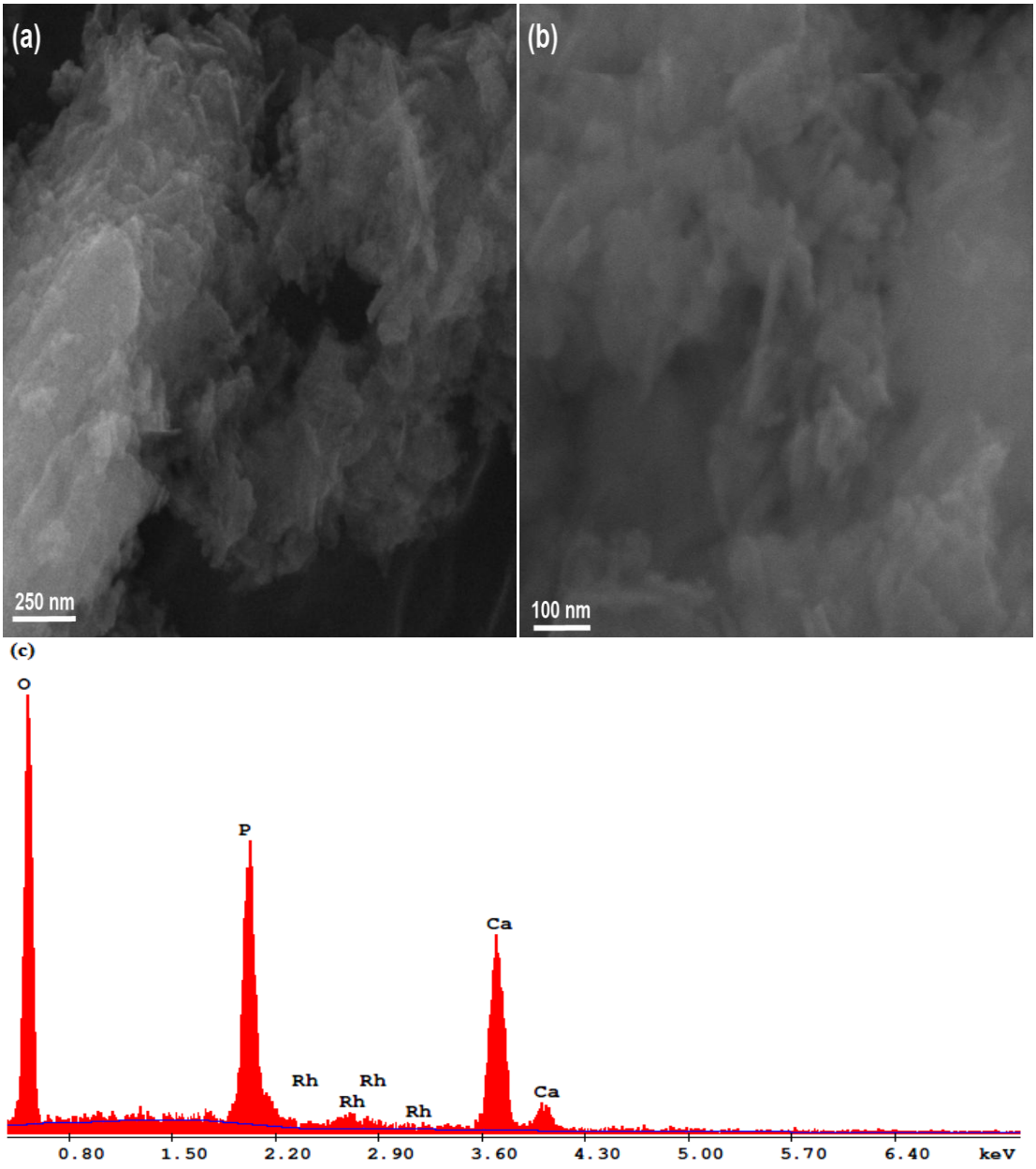

Figure 14. (a) and (b) are Scanning Electron Microscopy (SEM) images of the RhNPs@HAP sample in different magnifications. (c) SEM associated EDX spectrum of the RhNPs@HAP sample.

However, EDX analysis integrated with SEM indicates the existence of rhodium in the sample. The SEM-EDX spectrum given in Figure 14c exhibits the $L_{\alpha 1}$, $L_{\beta 1}$, L_{b1}, L_{b2}, and L_{g1} lines for Rh at 2.7, 2.8, 2.85, 3.0 and 3.2 keV, respectively [105].

One of the most efficient methods in characterization of the metal nanoparticles is the transmission electron microscopy (TEM) that gives information about size, shape, and size distribution of nanoparticles. Figure 15 depicts the TEM images of rhodium(0) nanoparticles supported on hydroxyapatite. From the inspection of TEM images given in Figure 15, one can conclude that the well dispersed rhodium(0) nanoparticles are formed on the surface of hydroxyapatite support.

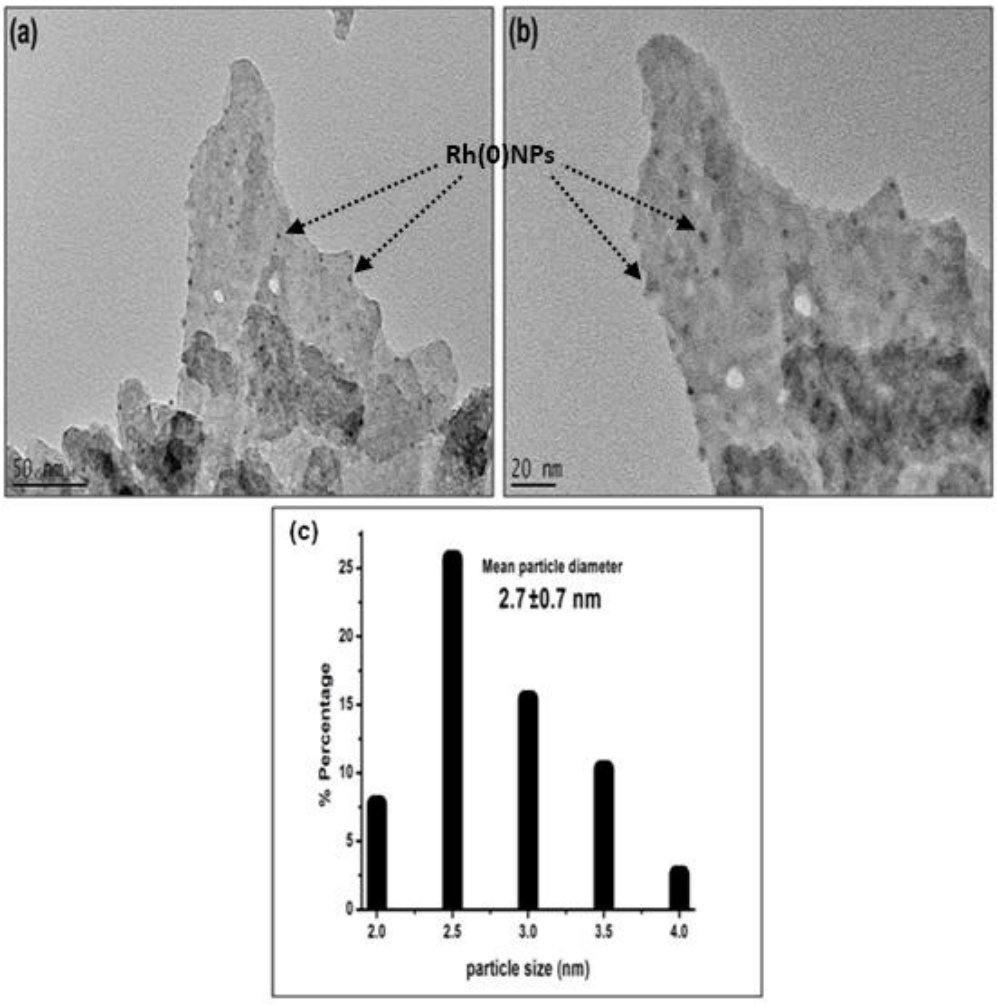

Figure 15. (a) and (b) are Transmission Electron Microscopy (TEM) images of RhNPs@HAP in different magnifications, (c) corresponding particle size histogram of RhNPs@HAP.

The particle sizes of 50 untouching particles in the TEM images given in Figure 15a and b were measured in order to construct the histogram. Thus, the particle size of the Rh(0) nanoparticles were calculated. As determined from the histogram given in Figure 15c, the mean particle size of rhodium(0) nanoparticles is 2.7 ± 0.7 nm.

For the further confirmation of rhodium(0) nanoparticles on hydroxyapatite, TEM-EDX characterization technique was also performed from the different range of the sample. The TEM-EDX spectrum of the RhNPs@HAP sample given in Figure 16 shows the existence of rhodium as the sole element in addition to the framework elements of the hydroxyapatite (Ca, P, and O) and also Cu from TEM grid.

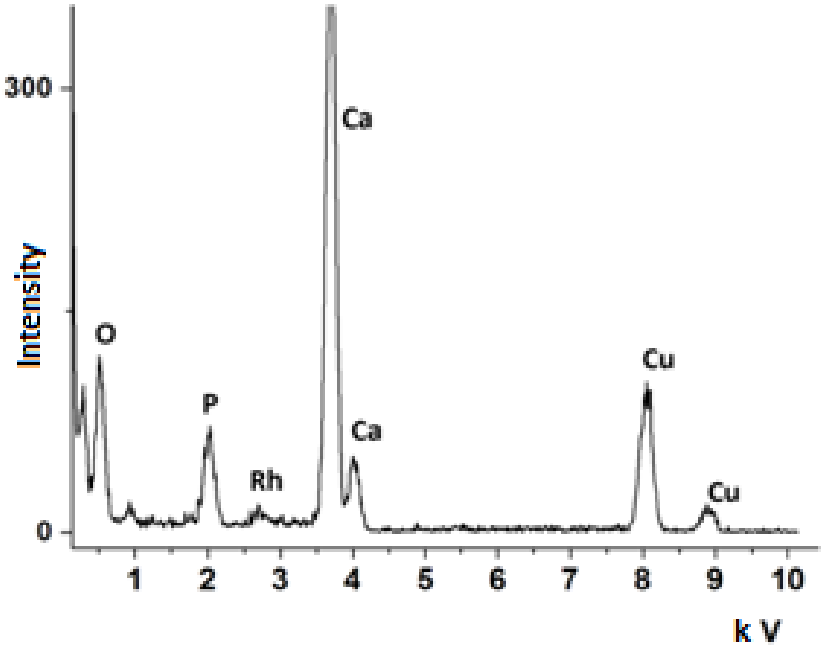

Figure 16. TEM-EDX spectrum of rhodium(0) nanoparticles supported on hydroxyapatite.

Nitrogen adsorption-desorption isotherms of the rhodium(0) nanoparticles supported on hydroxyapatite sample are given in Figure 17. One observes the isotherms of type III which is characteristic for materials having non-porosity [106].

Brunauer-Emmett-Teller surface area of RhNPs@HAP was determined to be 53.0 $m^2.g^{-1}$, which is lower than that of the parent HAP (69.3 $m^2.g^{-1}$). When passing from hydroxyapatite to rhodium(0) nanoparticles supported on hydroxyapatite, the surface area is decreased from 69.3 to 53.0 $m^2.g^{-1.}$ This is another piece of evidence for the presence of rhodium(0) nanoparticles adsorbed on the HAP surface. Furthermore, no hysteresis loop was observed in the N_2 adsorption-desorption isotherm of rhodium(0) nanoparticles supported on hydroxyapatite indicating that the procedure followed in the preparation of rhodium(0) nanoparticles supported on hydroxyapatite does not create any mesopores.

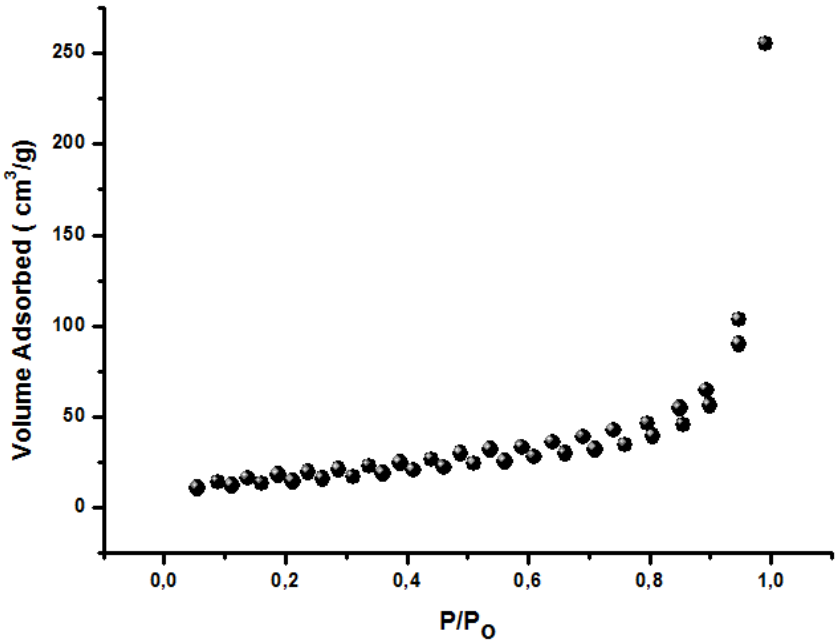

Figure 17. Nitrogen adsorption- desorption isotherm of rhodium nanoparticles supported on hydroxyapatite (with rhodium content of 0.99. %wt.)

The oxidation state of rhodium and the surface composition of the RhNPs@HAP sample were investigated by X-ray photoelectron spectroscopy (XPS). The survey-scan XPS spectrum of the RhNPs@HAP sample Figure 18d indicates that rhodium is the only element detected in the sample in addition to the framework elements of hydroxyapatite (Ca, P, and O). The high resolution Rh 3d XPS spectrum of the RhNPs@HAP sample is given in the Figure 18a. This spectrum shows two

prominent bands at 310 and 314.4 eV, readily assigned to Rh(0) $3d_{5/2}$ and Rh(0) $3d_{3/2}$, respectively [107]. This observation confirms the reduction of Rh^{+3} ions to rhodium(0) on the surface of hydroxyapatite during the hydrolysis of hydrazine-borane. Besides, the high resolution Ca 2p and P 2p XPS spectra of the framework elements are also shown in Figure 18b and c, respectively. These bands readily assigned to Ca 2p and P 2p in oxidation states +2 and +5, respectively [108,109].

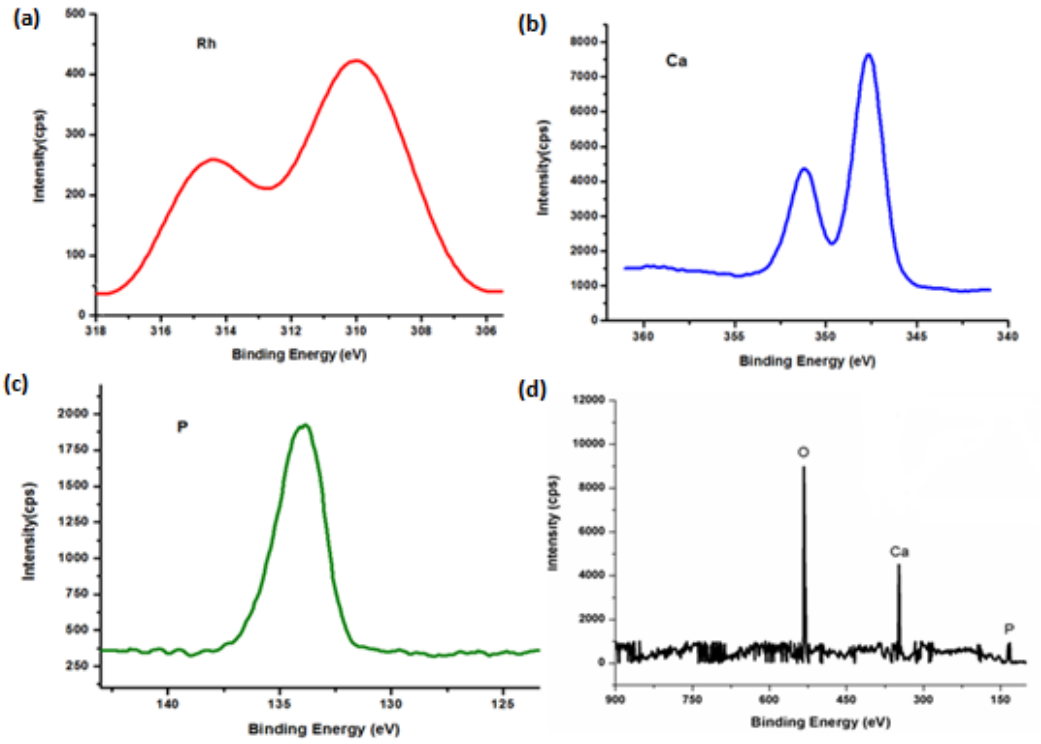

Figure 18. (a), (b), (c) X-Ray photoelectron (XPS) high resolution spectra of RhNPs@HAP for Rh 3d, Ca 2p and P 2p. (d) XPS survey scan of RhNPs@HAP.

5.2. Catalytic Activity of Rhodium(0) Nanoparticles Supported on Hydroxyapatite in Hydrogen Generation from the Hydrolysis of Hydrazine-Borane and Ammonia-Borane

5.2.1. Catalytic Activity of Rhodium(0) Nanoparticles Supported on Hydroxyapatite in the Hydrolysis of Hydrazine-Borane.

After the preparation and characterization of the well-dispersed rhodium(0) nanoparticles supported on hydroxyapatite, they were employed as catalyst in the

hydrolysis of hydrazine-borane and ammonia-borane. Before studying the catalytic activity of RhNPs@HAP, one has to check the impact of hydroxyapatite on the hydrolysis reaction. In order to check whether the hydroxyapatite matrix catalyzes the hydrogen generation from the hydrolysis of hydrazine-borane and ammonia-borane, the hydrolysis reaction was performed at various temperatures (20, 25, 30, 35, 40 °C) in the presence of hydroxyapatite. This control experiment showed that the support material is catalytically inactive in hydrogen generation from the hydrolysis of hydrazine-borane and ammonia-borane.

In the next step, kinetics of hydrolysis reaction of hydrazine-borane in the presence of RhNPs@HAP was investigated in order to obtain the rate law for the reaction and also activation parameters. For this purpose, first of all, various concentrations of rhodium from the Rh^{+3}-exchanged hydroxyapatite sample with rhodium loading of 0.99 % wt. were examined for the hydrolysis of 100 mM hydrazine-borane solution at 25.0 ± 0.1 °C. The plots of stoichiometric ratio of H_2 evolved to hydrazine-borane *versus* time are given in Figure 19a for the hydrolysis of hydrazine-borane of 100 mM in the presence of RhNPs@HAP in various rhodium concentrations (0.05, 0.1, 0.2, 0.4, 0.6 mM Rh) at 25.0 ± 0.1 °C. Even if the concentration of the rhodium is very low (0.05 mM Rh), the rapid hydrogen generation starts immediately without induction time with exceptional initial TOF value of 21280 h^{-1}. The hydrogen generation continues almost linearly until the complete hydrolysis of hydrazine-borane yields in 3 equivalents of H_2. The hydrogen generation rate was determined from the linear portion of the each plot for the hydrolysis reaction performed starting with different catalyst concentrations. The hydrogen generation rate changes between 4.8 - 28.8 mL H_2/ min even at low concentrations (0.05-0.60 mM Rh) at 25.0 ± 0.1 °C. Figure 19b shows the plot of the hydrogen generation rate *versus* rhodium concentrations both in logarithmic scales. This plot gives straight line with a slope of 0.75. Thus, the catalytic hydrolysis of hydrazine-borane is 0.75 order with respect to rhodium concentration.

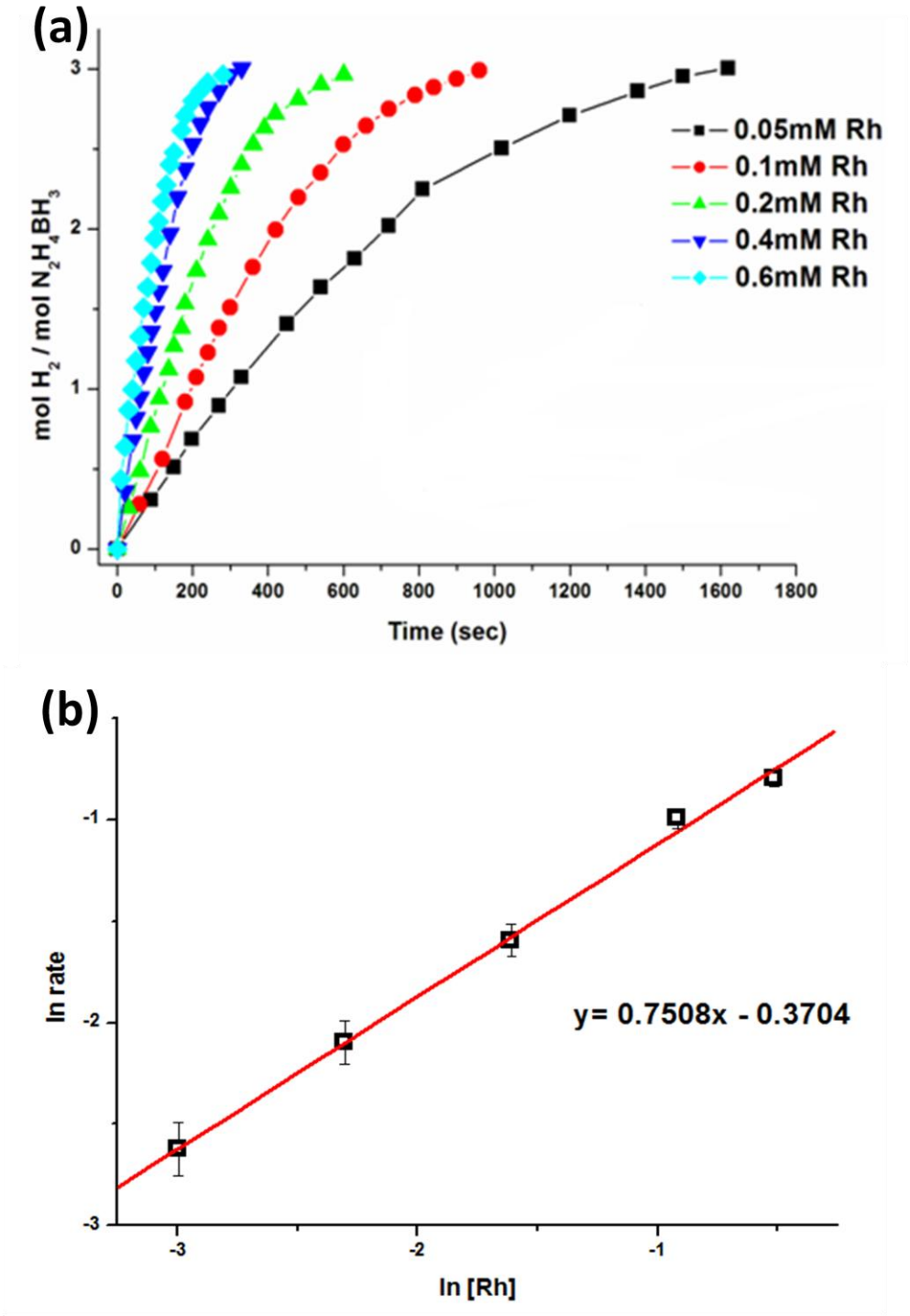

Figure 19. (a) Plot of mol H_2/mol $N_2H_4BH_3$ *versus* time (sec) for the hydrolysis of hydrazine-borane starting with Rh^{3+}@HAP (with a rhodium content of 0.99 % wt) in different Rh concentrations [Rh] = 0.05, 0.1, 0.2, 0.4, 0.6 mM at 25.0 ± 0.1 ˚C. (b) Plot of hydrogen generation rate *versus* the concentration of rhodium (both in logaritmic scale.)

The next step in kinetic studies is to find the effect of substrate concentration on the rate of hydrogen generation. For this purpose, various concentrations of hydrazine-borane between 50 and 800 mM were studied with the fixed concentration of 0.5 mM Rh that is in the form of Rh^{+3}-exchanged hydroxyapatite with a rhodium loading of 0.99 % wt. at 25.0 ± 0.1 ˚C. The plots of stoichiometric ratio of H_2 evolved to hydrazine-borane *versus* time are exhibited in Figure 20a for the hydrolysis of hydrazine-borane in various concentrations (50, 100, 150, 200, 400, 600, 800 mM) starting with Rh^{+3}-exchanged hydroxyapatite [Rh= 0.5 mM] at 25.0 ± 0.1 °C. Even if the ratio between substrate and catalyst is very high (max. 1600 in our conditions), the fast hydrogen generation begins without induction time. The hydrogen generation proceeds almost linearly until 3 equivalents H_2 are evolved. The hydrogen generation rate was determined from the linear portion of the each plot for the hydrolysis reaction of hydrazine-borane performed starting with different substrate concentrations. The hydrogen generation rate increases with the increasing substrate concentration. Figure 20b exhibits the plot of hydrogen generation rate *versus* substrate concentrations both in logarithmic scales. The logarithmic graph has the line with the slope of 0.5. Thus, catalytic hydrolysis of hydrazine-borane progresses 0.5 order with respect to the substrate concentration.

The results of the kinetic studies can be used to establish the rate law of the catalytic hydrolysis of hydrazine-borane;

$$-\frac{d[N_2H_4BH_3]}{dt} = +\frac{d[H_2]}{3dt} = k_{obs}[Rh]^{0.75}[N_2H_4BH_3]^{0.50} \qquad (8)$$

In order to find activation parameters, temperature dependence of the hydrolysis reaction of hydrazine-borane catalyzed by *in-situ* generated RhNPs@HAP was studied at the various temperature in the range of 20-40 °C using the constant concentration of hydrazine-borane ([HB]=100 mM) and rhodium ([Rh]=0.25 mM) starting with a Rh^{+3}-exchanged hydroxyapatite. The stoichiometric ratio of H_2 evolved to hydrazine-borane *versus* time is plotted in Figure 21a for the hydrolysis reaction of hydrazine-borane catalyzed by RhNPs@HAP at the different temperatures. The rapid hydrogen generation starts without induction time even at

low temperatures. The rate constant of each reaction was determined from the linear portions of the each plot for the hydrolysis of hydrazine-borane catalyzed by *in-situ* generated RhNPs@HAP at the different temperatures. The values of rate constant were used to find activation parameters by using Arrhenius [110] and Eyring [111] equations in order to calculate Arrhenius activation energy E_a = 45 kJ/mol, activation enthalpy $\Delta H^{\#}$ = 42 kJ/mol, and activation entropy $\Delta S^{\#}$ = -113 J/mol·K. (Figure 21b-c).

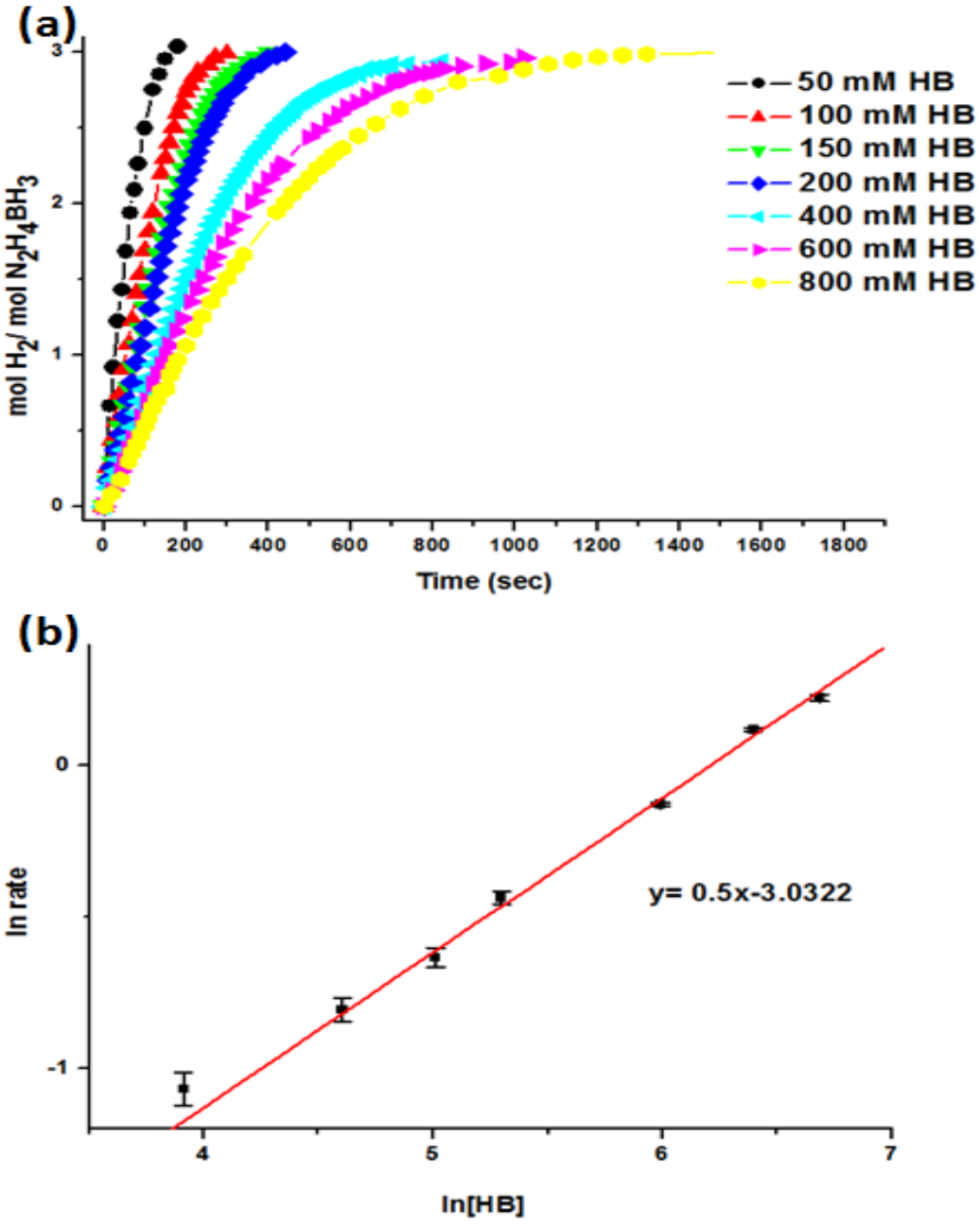

Figure 20. (a) Plot of mol H_2/mol $N_2H_4BH_3$ *versus* time (sec) for the hydrolysis of hydrazine-borane in various concentrations [$N_2H_4BH_3$] = 50, 100, 150, 200, 400, 600, 800 mM starting with Rh^{3+}@HAP (with a rhodium content of 0.99 % wt) [Rh] = 0.5 mM at 25.0 ± 0.1 ˚C. (b) Plot of the hydrogen-generation rate *versus* the substrate concentration (both in logarithmic scale) in the hydrolysis of $N_2H_4BH_3$ catalyzed by *in-situ* generated RhNPs@HAP at 25.0 ± 0.1 ˚C.

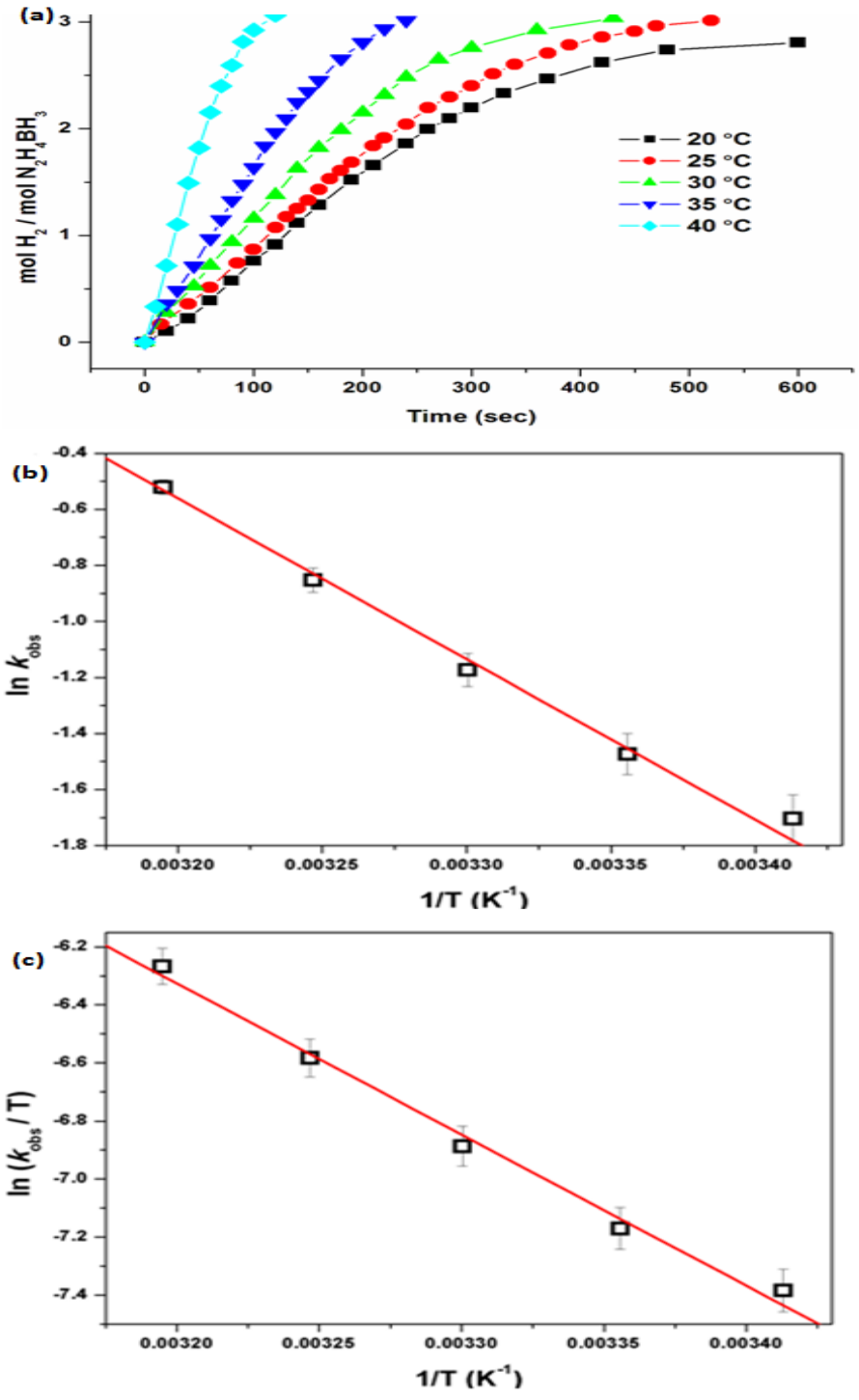

Figure 21. (a) Plot of mol H_2/mol $N_2H_4BH_3$ *versus* time (sec) for the hydrolysis of hydrazine-borane [$N_2H_4BH_3$] = 100 mM starting with Rh^{3+}@HAP (with a rhodium content of 0.99 % wt) [Rh] = 0.25 mM at 20- 40˚C. (b) Arrhenius plot, (c) Eyring plot for the hydrolysis of hydrazine-borane

5.2.1.1. Catalytic Lifetime and Reusability of Rhodium(0) Nanoparticles Supported on Hydroxyapatite in the Hydrolysis of Hydrazine-Borane

The lifetime of RhNPs@HAP catalyst was determined by measuring the total turnover number in the hydrogen generation from the hydrolysis of hydrazine-borane. Such a lifetime experiment was started by adding Rh^{+3}-exchanged hydroxyapatite including 43 μmol rhodium and 4.0 mmol hydrazine-borane into the 10 mL water at 25.0 ± 0.1°C. After the liberation of 3 equivalents H_2 gas, a new batch of hydrazine-borane was added to reaction flask and hydrogen generation was followed. This procedure was repeated until no more gas evolution was seen. At the end of the experiment, approximately 8.5 mmol hydrazine-borane were used. The catalytic lifetime of the RhNPs@HAP was calculated to be 52850 total turnovers in the hydrolysis of hydrazine-borane over 27 h reaction before deactivation at 25.0 ± 0.1°C.

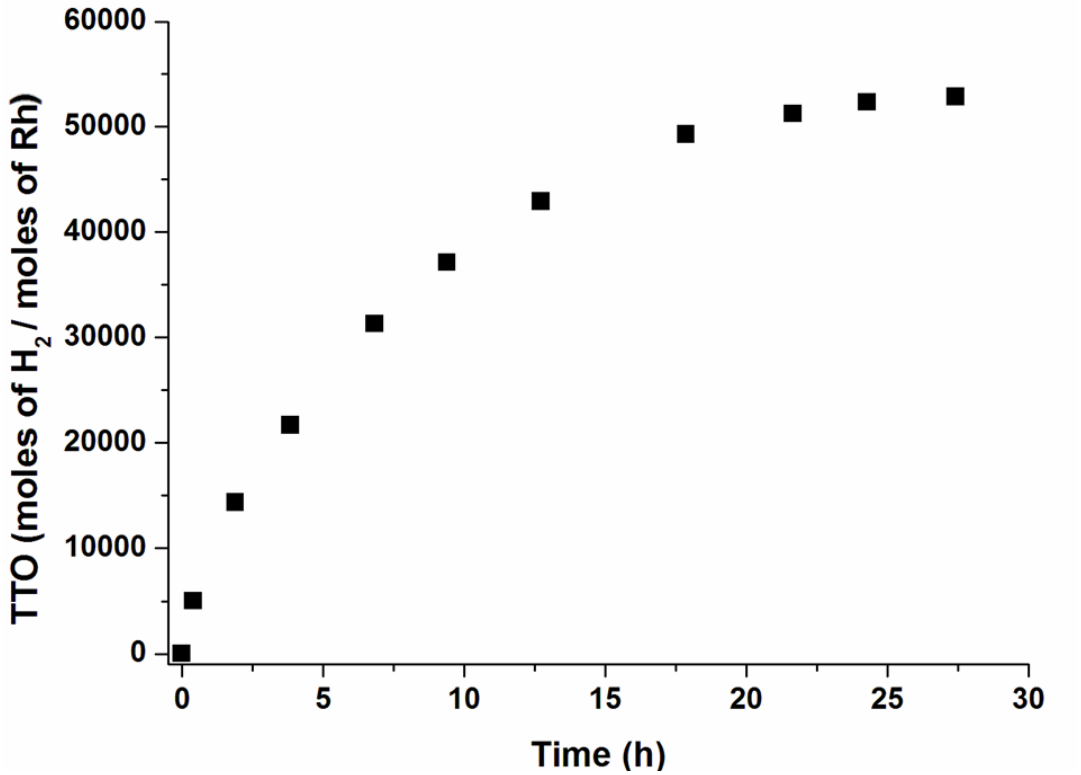

Figure 22. Graph of total turnover number (TTO) *versus* time for the hydrolysis of hydrazine-borane ($N_2H_4BH_3$) starting with Rh^{3+}@HAP (with a rhodium content of 0.99 % wt) at 25.0 ± 0.1 ˚C.

The main advantages of the heterogeneous catalyst compared to homogeneous catalyst in the industrial and chemical applications are their isolability and reusability properties. Therefore, the reusability of rhodium(0) nanoparticles supported on hydroxyapatite was tested in the hydrolysis of hydrazine-borane. For this purpose, after 3 equivalents hydrogen generation from 100 mM hydrazine-borane started with Rh^{+3}-exchanged hydroxyapatite ([Rh]= 0.48 mM), the catalyst was isolated as black powders from reaction solution by centrifugation at 10000 rpm, washed with copious amount of water, then dried under vacuum. The isolated RhNPs@HAP sample was redispersed in water and used in the hydrolysis of 100 mM hydrazine-borane. The catalytic activity was measured as the hydrogen generation rate. The same procedure was repeated five times and the results are illustrated in Figure 23. The catalytic activity of RhNPs@HAP in the hydrolysis of hydrazine-borane decreases slightly in successive runs. The slight decrease in catalytic activity in subsequent runs may be due to the material loss during the isolation and redispersing procedure or due to passivation of nanoclusters surface by increasing amount of boron products, e.g. borate anion, which might decrease the accessibility of active sites for hydrazine-borane. Additionally, the clumping of rhodium nanoparticles throughout the catalytic runs might also lead to deactivation of RhNPs@HAP. It is crucial to say that, RhNPs@HAP show high activity in the reusability test by retaining 62 % of their initial activity with > 99 % conversion even at its fifth reuse in the hydrolysis of hydrazine-borane. This valuable result is the evidence of the reusability, bottlability and isolability of RhNPs@HAP catalyst.

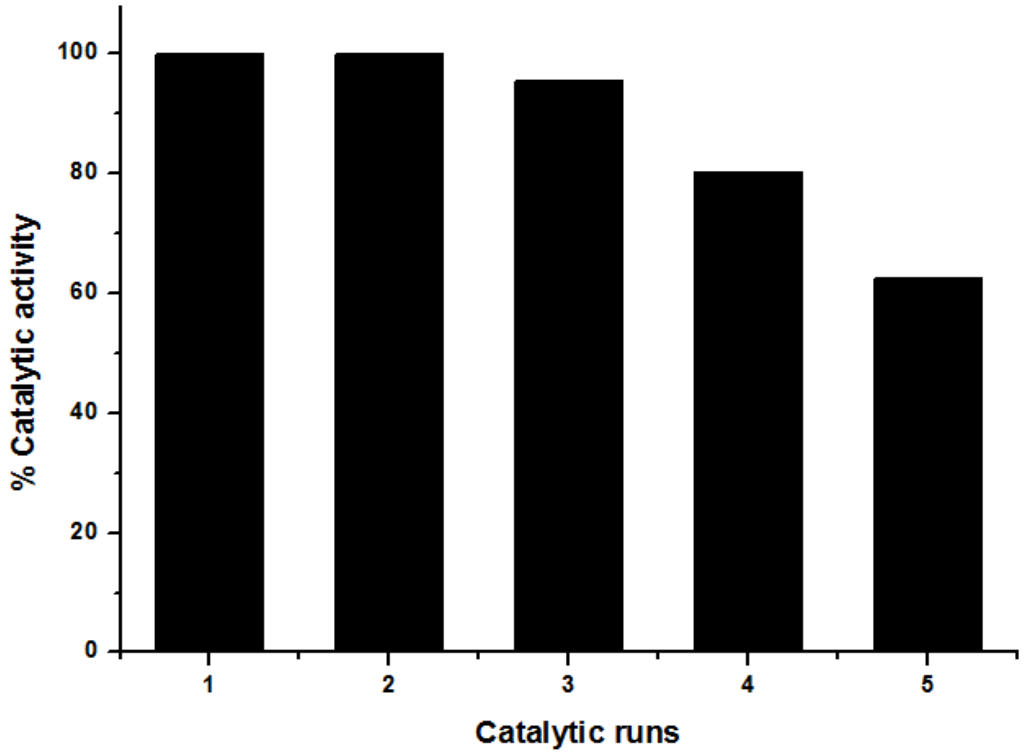

Figure 23. Percentage catalytic activity of RhNPs@HAP in each run of hydrolysis of hydrazine-borane ([HB]=100 mM).

5.2.2. Catalytic Activity of Rhodium(0) Nanoparticles Supported on Hydroxyapatite in the Hydrolysis of Ammonia-Borane.

In the next part, the catalytic activity of RhNPs@HAP was examined in hydrolysis reaction of another boron-based compound, ammonia-borane. The catalytic experiments of ammonia-borane were studied using the preformed catalyst. Rhodium(0) nanoparticles supported on hydroxyapatite was formed at the end of hydrolysis reaction of 100 mM hydrazine-borane. The catalyst was separated from reaction solution by centrifugation, washed with great amount of water and dried under vacuum. Isolated RhNPs@HAP was kept under inert gas atmosphere.

In order to determine rate law of hydrolysis reaction of ammonia-borane, first of all, the effect of rhodium concentration starting with RhNPs@HAP on the hydrogen generation rate was studied in the presence of 100 mM ammonia-borane at

25.0 ± 0.1 °C. Figure 24a shows the stoichiometric ratio of H_2 generated to NH_3BH_3 *versus* time for the hydrolysis of ammonia-borane (100 mM) in the presence of RhNPs@HAP in different rhodium concentrations (0.05, 0.10, 0.20, 0.40, and 0.80 mM) at 25.0 ± 0.1°C. Due to the use of preformed catalyst, the hydrolysis reaction starts rapidly without induction time even at low concentration of rhodium (0.05 mM). The hydrogen generation continues almost linearly until 3 equivalents H_2 are evolved. The linear portions of each plot for the hydrolysis reaction of ammonia-borane in different catalyst concentrations were used to determine hydrogen generation rate. The rates of hydrogen evolution are in the range of 1.1–36.8 mL H_2/min. Figure 24b depicts the plot of hydrogen generation rate *versus* the concentration of rhodium both in logarithmic scale. This plot gives a straight line with a slope of approximately 1.0. Therefore, RhNPs@HAP catalyzed hydrolysis of ammonia-borane is first order with respect to the rhodium concentration.

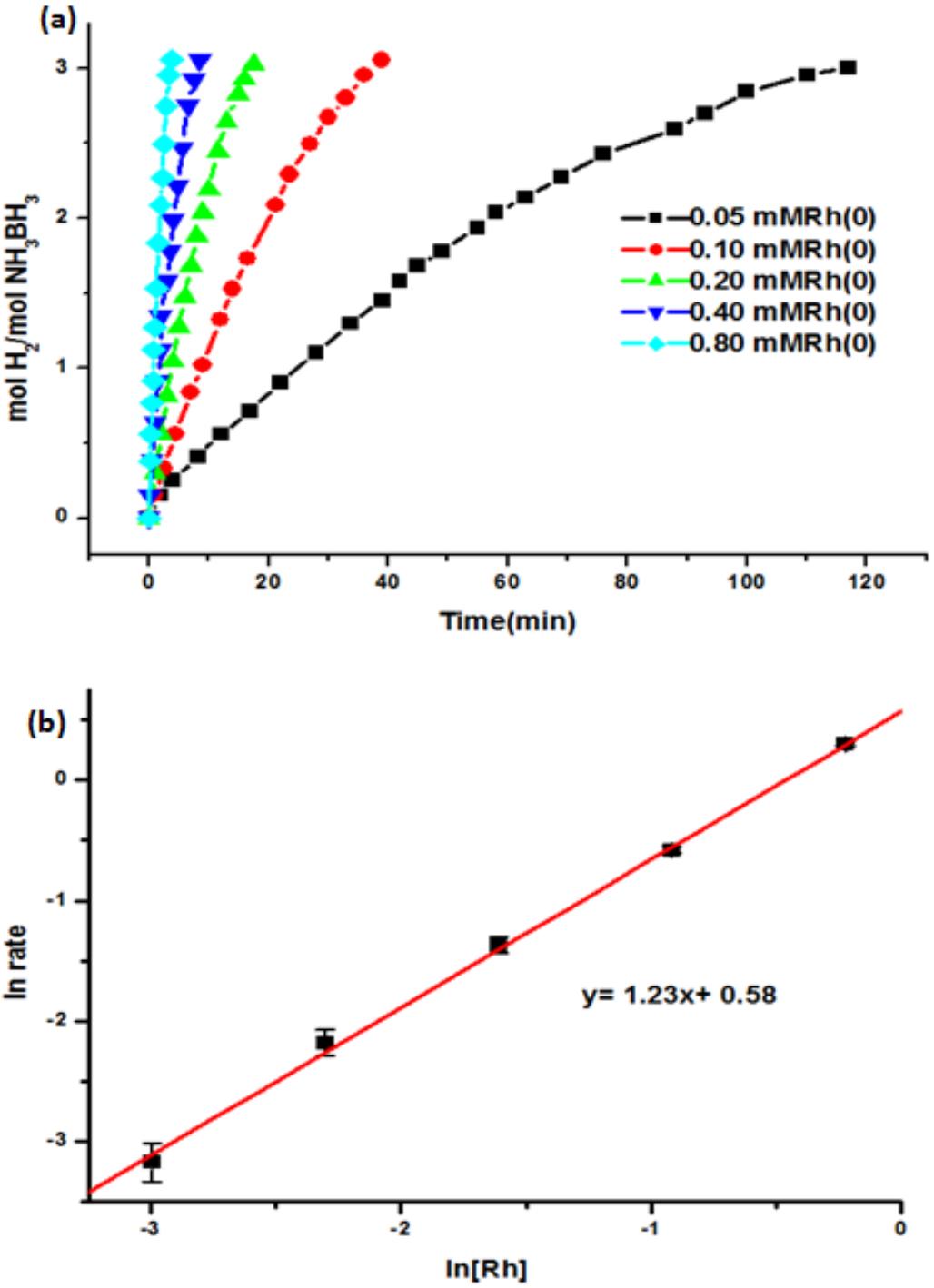

Figure 24. (a) Plot of mol H_2/mol NH_3BH_3 *versus* time (min) for the hydrolysis of ammonia-borane starting with RhNPs@HAP (with a rhodium content of 0.99 % wt.) in different Rh concentrations [Rh] = 0.05, 0.1, 0.2, 0.4, 0.8 mM at 25.0 ± 0.1 ˚C. (b) Plot of hydrogen generation rate *versus* the concentration of rhodium (both in logaritmic scale.)

The next step is the studying the effect of substrate concentration on the hydrogen generation rate. For this purpose, the initial concentration of ammonia-borane was altered in the range of 50-300 mM by keeping the catalyst concentration constant at 0.5 mM Rh in the hydrogen generation from the hydrolysis of ammonia-borane at 25.0 ± 0.1°C. The graph of stoichiometric ratio of H_2 generated to NH_3BH_3 *versus* time is exhibited in the Figure 25a for the hydrolysis of ammonia-borane in various concentrations (50, 100, 150, 200, and 300 mM) initiating with RhNPs@HAP, [Rh] = 0.5 mM at 25.0 ± 0.1 °C. The rapid hydrogen generation is observed in the hydrolysis of ammonia-borane in various substrate concentrations. The hydrogen generation rate was determined form the linear portions of each plot for different ammonia-borane concentrations catalyzed by preformed RhNPs@HAP. Figure 25b shows the plot of hydrogen generation rate *versus* the concentration of ammonia-borane both in logaritmic scale. The slope of straight line is approximately zero which specifies that the catalytic hydrolysis of ammonia-borane is zero order with respect to the substrate concentrations. The rate law of reaction can be written as followed equation;

$$-\frac{d[NH_3BH_3]}{dt} = +\frac{d[H_2]}{3dt} = k_{obs}[Rh] \qquad (9)$$

In order to find the activation parameters, the hydrolysis reactions of ammonia-borane were performed at various temperatures (20, 25, 30, 35, and 40 °C) using the constant concentration of ammonia-borane ([AB] = 100mM) and rhodium ([Rh] = 0.25 mM) in the presence of RhNPs@HAP. Figure 26a exhibits the plot of stoichiometric ratio of H_2 generated to NH_3BH_3 *versus* time for the hydrolysis of 100 mM ammonia-borane starting with RhNPs@HAP including 0.25 mM Rh. The rate constant was determined from the linear part of the each plots of Figure 26a for the hydrolysis of ammonia-borane at five different temperatures in order to construct the Arrhenius (Figure 26b) and Eyring (Figure 26c) plots to specify activation energy (E_a=43.1 kJ/mol), activation enthalpy ($\Delta H^{\#}$ =39.7 kJ/mol) and the activation entropy ($\Delta S^{\#}$ = -89.7 J/K·mol) for RhNPs@HAP catalyzed hydrolysis of AB, respectively.

Additionally, the small activation enthalpy and the large negative activation entropy values are strongly indicative of an associative mechanism in transition state for the catalytic hydrolysis of both hydrazine-borane and ammonia-borane as in the case of the metal catalyzed hydrolysis of sodium borohydride [112] or ammonia-borane [113].

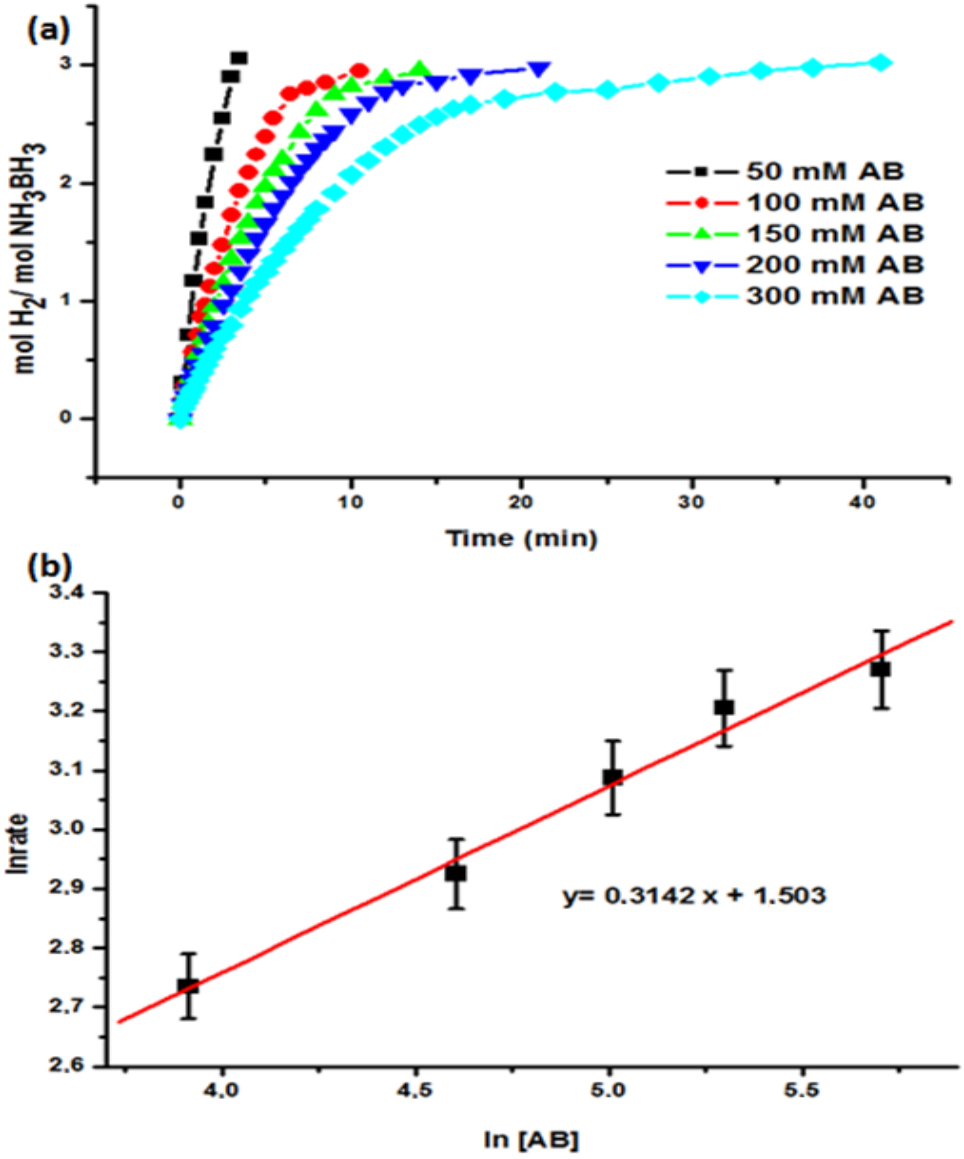

Figure 25. (a) Plot of mol H_2/mol NH_3BH_3 *versus* time (min) for the hydrolysis of ammonia-borane in various concentrations [NH_3BH_3] = 50, 100, 150, 200, 300 mM starting with RhNPs@HAP (with a rhodium content of 0.99 % wt.) [Rh] = 0.5 mM at 25.0 ± 0.1 ˚C. (b) Plot of the hydrogen-generation rate *versus* the substrate concentration (both in logarithmic scale).

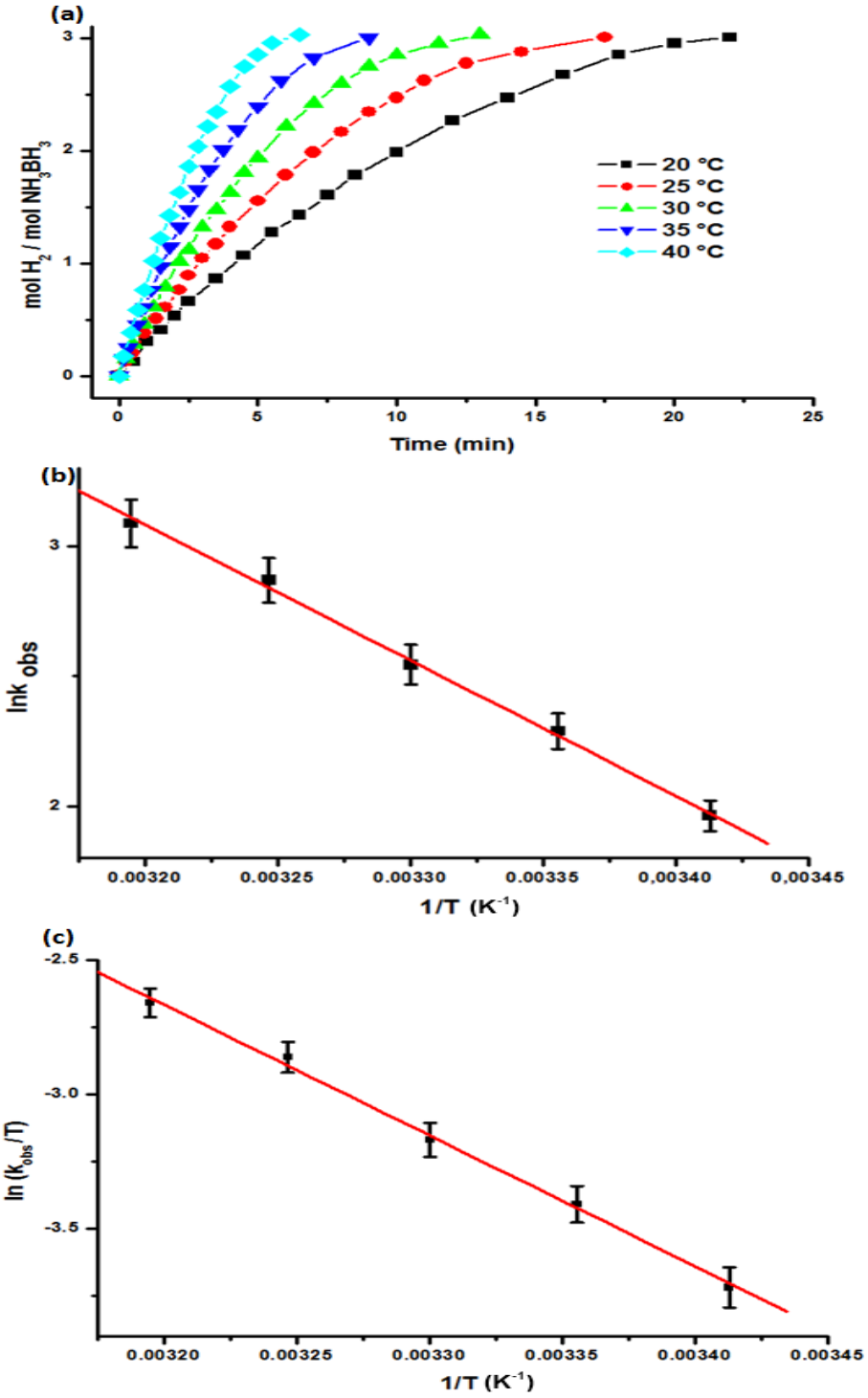

Figure 26. (a) Plot of mol H_2/mol NH_3BH_3 *versus* time (min) for the hydrolysis of ammonia-borane [NH_3BH_3] = 100 mM starting with RhNPs@HAP (with a rhodium content of 0.99 % wt) [Rh] = 0.25 mM at 20 - 40˚C. (b) Arrhenius plot, (c) Eyring plot for the hydrolysis of ammonia-borane.

5.2.2.1. Catalytic Lifetime of Hydroxyapatite Supported Rhodium(0) Nanoparticles in the Hydrolysis of Ammonia-Borane

The lifetime experiment of the RhNPs@HAP catalyst was carried out by measuring the total turnover number in the hydrolysis of ammonia-borane. The lifetime experiment was initiated with 1.0 mmol substrate in the presence of RhNPs@HAP including 46 μmol Rh in 10 mL water at 25.0 ± 0.1 ˚C. After 3 equivalents H_2 generation, a new batch of ammonia-borane was added into the reaction flask and the reaction was continued until no hydrogen gas evolution was observed. At the end of this experiment, approximately 2.5 mmol ammonia-borane were used. RhNPs@HAP provide 14250 total turnovers in the hydrolysis of ammonia-borane over 12 h reaction before deactivation at 25.0 ±0.1.˚C (Figure 27).

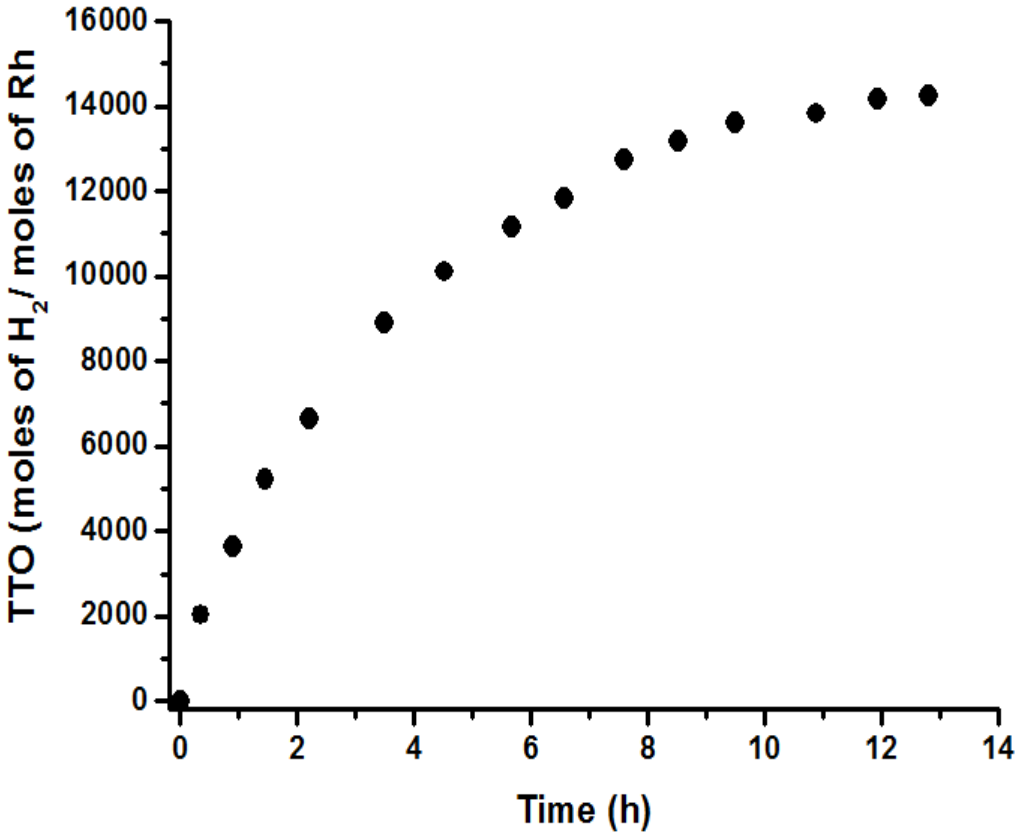

Figure 27.Graph of total turnover number (TTO) *versus* time for the hydrolysis of ammonia-borane (NH_3BH_3) starting with RhNPs@HAP (with a rhodium content of 0.99 % wt.) at 25 ± 0.1 ˚C.

CHAPTER 6

CONCLUSIONS

To sum up, the main findings of this dissertation about preparation, characterization of rhodium(0) nanoparticles supported on hydroxyapatite and their catalytic employment in hydrogen generation from the hydrolysis of hydrazine-borane and ammonia-borane can be outlined as follows;

- Rhodium(0) nanoparticles supported on hydroxyapatite was prepared by utilizing applicable procedure that is the simple ion-exchange followed by *in-situ* reduction of Rh^{+3} ions to rhodium(0) during the hydrolysis of the hydrazine-borane.
- This isolable and reusable catalyst was characterized thoroughly by the various characterization methods including ICP-OES, SEM, TEM, EDX, XRD, XPS, and N_2 adsorption-desorption. All the results show the formation of well-dispersed rhodium(0) nanoparticles supported on hydroxyapatite.
- These well dispersed rhodium(0) nanoparticles having mean particle size of 2.7 ± 0.7 nm formed *in-situ* during the hydrolysis reaction were quite active in the hydrolysis of hydrazine-borane. Additionally, they retain their initial high activity in the second use as catalyst in another boron-based compound, ammonia-borane.
- RhNPs@HAP provide over 52850 total turnovers 27 h and an initial high turnover frequency value of TOF= 6700 h^{-1} in the hydrolysis of hydrazine-borane. They provide 14250 total turnovers over 12 h in the hydrolysis of ammonia-borane.
- RhNPs@HAP are isolable, bottable and redispersable. In the reusability experiments, they show high activity with 3 equivalents H_2 generation from hydrazine-borane retaining 62 % of their initial activity at the fifth run.
- The results of kinetic experiments of RhNPs@HAP catalyzed hydrolysis of hydrazine-borane shows that hydrolysis of hydrazine-borane is 0.75 order

with respect to rhodium concentration and 0.5 order with respect to hydrazine-borane concentration.

- According to rate law of hydrolysis reaction of ammonia-borane catalyzed by RhNPs@HAP, hydrolysis reaction progresses first order with respect to rhodium concentration and zero order with respect to ammonia-borane concentration.

Owing to the high catalytic activity, easy preparation, isolability, bottlability, and reusability of rhodium(0) nanoparticles supported on hydroxyapatite, RhNPs@HAP can be considered as a catalyst in the applications of hydrolysis reactions of boron-based compounds for the fuel-cell applications. Hydrazine-borane and ammonia-borane should be considered as the efficient materials for hydrogen storage that is still the challenging issue of "hydrogen economy".

REFERENCES

[1] Gregory, D.P., *Division of Fuel Chemistry*, **1974**, 19, 93.

[2] Sartbaeva, A., Kuznetsov, V.L., Wells, S. A., Edwards, P. P., *Energy and Environ.*, **2008**, 1, 79.

[3] Strub, A. A, Imarisio, G., *Hydrogen as an Energy Vector*, Comission of the European Communities, D. Reidel Publishing Co., Dordrecht, **1980**.

[4] Alfenso, E. Y., Beaird, A. M., Davis, T.,Matthews, M. A., *Ind. Eng. Chem. Res.*, **2009**, 48, 3703.

[5] Chen, P., Xiong, Z.T., Luo, J.Z., Lin, J.Y., Tan, K.L., *Nature*, **2002**, 420, 302.

[6] Bacsa, R., Laurent, C., Morishima, R., Suzuki, H., Lelay, M., *J Phys Chem B*, **2004**,108, 12718.

[7] Lim, S.H., Luo, J.Z., Zhong, Z.Y., Ji, W., Lin, J.Y., *Inorg. Chem.*, **2004**, 44, 4124.

[8] Dong, J.X., Wang, X.Y., Xu, H,, Zhao, Q., Li, J.P., *Int. J. Hydrogen Energy*, **2007**, 32, 4998.

[9] McKeown, N.B., Budd, P.M., *Chem. Soc. Rev.*, **2006,** 35, 675.

[10] Rood, J.A., Noll, B.C., Henderson, K.W., *Inorg. Chem.*, **2006,** 45, 5521.

[11] Scheideman, M., Wang, G.Q., Vedejs, E., *J. Am .Chem. Soc.*, **2008**, 130, 8669.

[12] Sakintuna, B., Lamari-Darkrim, F., Hirscher, M., *Int. J. Hydrogen Energy*, **2007**, 32, 1121.

[13] (a) Chandra, M., Xu, Q., *J. Power Sources*, **2006**, 156,190. (b) Chandra, M., Xu, Q., *J. Power Sources*, **2006**, 159, 855. (c) Xu, Q., Chandra, M., *J. Power Sources*, **2006**, 163, 364. (d) Chandra, M., Xu, Q., *J. Power Sources*, **2007**, 168, 135. (e) Zahmakiran, M., Özkar, S., *Appl. Catal. B*, **2009**, 89, 104. (f) Durap, F., Zahmakıran, M., Özkar, S., *Int. J. Hydrogen Energy*, **2009**, 34, 7223. (g) Durap, F., Zahmakıran, M., Özkar, S., *Appl. Catal. A*, **2009**, 369, 53. (h) Zahmakıran, M., Durap, F., Özkar, S., *Int. J. Hydrogen Energy*, **2010**, 35, 187. (i) Zahmakıran, M., Ayvalı, T., Akbayrak, S., Çalışkan, S., Çelik, D., Özkar, S., *Catal. Today*, **2011**, 170, 76. (j)

Yan, J.M., Zhang, X.B., Han, S., Shioyama, H., Xu, Q., Inorg. Chem., **2009**, 48, 7389.

[14] (a) Karahan, S., Zahmakıran, M., Özkar, S., *Int. J. Hydrogen Energy*, **2011**, 36, 4958. (b) Çelik, D., Karahan, S., Zahmakıran, M., Özkar, S., *Int. J. Hydrogen Energy*,**2012**, doi:10.1016j.ijhydene.2011.12.067.

[15] Energy Information Administration, Annual Energy Outlook 2005 With Projections To 2025, www.eia.doe.gov/oiaf/aeo/pdf/0383(2005).pdf, February, **2005**.

[16] (a) Wolf, G., Baumann, J., Baitalow, F., Hoffmann, F.P., *Thermochim. Acta*, **2003**, 19, 343. (b) Baumann, J., Baitalow, F., Wolf, G., *Thermochim. Acta*, **2005**, 9,450. (c) Gutowska, A., Li, L., Shin, Y., Wang, C.M., Li, X.S., Linehan, J.C., Smith, R.S., Kay, B.D., Schmid, B., Shaw, W., Gutowski, M., Autrey T., *Angew., Chem.*, **2005,** 44, 3578. (d) Benedetto, S.D., Carewska, M., Cento, C., Gislon, P., Pasquali, M., Scaccia, S., Prosini, P.P., *Thermochim. Acta*, **2006**, 441, 184.

[17] (a) Jaska, C.A., Temple, K., Lough, A.J., Manners, I., *J. Am. Chem. Soc.*, **2003,** 125, 9424. (b) Chen, Y., Fulton, J.L., Linehan, J.C., Autrey T., *J. Am. Chem. Soc.*, **2005,** 127, 3254

[18] Bluhm, M.E., Bradley, M.G., Butterick III, R., Kusari, U., Sneddon, L.G., *J. Am. Chem. Soc.*, **2006,** 128, 7748.

[19] Wang, J.S., Geanangel, R.A., *Inorg. Chim. Acta*, **1988**, 148,185.

[20](a) Stephens, F.H., Baker, R. T., Matus, M.H., Grant, D. J.,.Dixon, D. A, *Angew. Chem., Int. Ed.*, **2007**, 46, 746 (b) Miller, A. J. M., Bercaw, J. E., *Chem. Commun.*, **2010**, 46, 1709.

[21] (a) He, T., Xiong, Z., Wu, G., Chu, H., Wu, C., Zhang, T., Chen, P., *Chem. Mater.*, **2009,** 21, 2315. (b) Kalidindi, S. B., Joseph, J, Jagirdar, B. R., *Energy Environ. Sci.*, **2009**, 2, 1274 (c) Li, Y., Song, P., Zheng, J., Li, X., *Chem.–Eur. J.*, **2010**, 16, 10887 (d) He, T., Wang, J. H., Wu, G. T., Kim, H., Proffen, T., Wu, A. A., Li, W., Liu, T., Xiong, Z. T., Wu, C. Z., Chu, H. L., Guo, J. P., Autrey, T., Zhang, T., Chen, P., *Chem.–Eur. J.*, **2010**, 16, 12814.

[22] Himmelberger, D.W., Yoon, C.W., Bluhm, M. E. , Carroll, P. J., Sneddon, L. G., *J. Am. Chem. Soc.*, **2009**, 131, 14101.

[23] Hugle, T., Kuhnel, M.F., Lentz, D., J. Am. Chem. Soc. 2009, 131, 7444.

[24] Staubitz, A., Robertson, A. P. M., Manners, I., *Chem. Rev.* **2010,** 110, 4079.

[25] (a) Umegaki, T., Yan, J.M., Zhang, X. B., Shioyama, H., Kuriyama, N., Xu, Q,. *Int. J. Hydrogen Energy,* **2009**,2303. (b) Jiang, H. L., Singh, S. K., Yan, J. M., Xu, Q., *ChemSusChem*, **2010**, 3, 541. (c) Jiang, H. L., Xu, Q., *Catalysis Today,***2011**, 170, 56.

[26] Gates, B.C., *Catalytic Chemistry*; Academic Press: New York, **1992**.

[27] Thomas, J.M., Thomas, W.J., *Principles and Practice of Heterogeneous Catalysis*, VCH, New-York, **1997**.

[28] (a) Schmid, G., Maihack, V., Lantermann, F., Peschel, S., *J. Chem. Soc., Dalton Trans.*, **1996**, 589., (b) Doyle, A., Shaikhutdinov, S. K., Jackson, S. D., Freund, H. J., *Angew. Chem.*, **2003**, 42, 5240.

[29] (a) Tosheva, L., Valtchev, V. P., *Chem. Mater.*, **2005**, 17, 2494. (b) Kato, H., Minami, T., Kanazawa, T., Sasaki, Y. ,*Angew. Chem.,Int. Ed.*, **2004**, 43, 1251.

[30] Castillejos, E., Debouttire, P. J., Roiban, L., Solhy, A., Martinez, V., Kihn, Y., Ersen, O., Philippot, K., Chaudret, B., Serp, P., *Angew. Chem., Int. Ed.*, **2009**, 48, 2529.

[31] (a) Sayle, D. C., Doig, J. A., Parker, S. C., Watson, G. W., *J. Mater. Chem.*, **2003**, 13, 2078. (b) Haruta, M., *Catal. Today*, **1997**, 36, 153.

[32] (a) Shi, F., Zhang, Q., Ma, Y., He, Y., Deng, Y., *J. Am. Chem. Soc.*, **2005**, 127, 4182. (b) Graeser, M., Pippel, E., Greiner, A., Wendorff, J. H., *Macromolecules*, **2007**, 40, 6032.

[33] El-Shall, M. S., Abdelsayed, V., Khder, A. E. R. S., Hassan, H. M. A., El-Kaderi, H. M., Reich, T. E., *J. Mater. Chem.*, **2009**, 19, 7625.

[34] (a) Zahmakıran, M., Özkar, S., *Langmuir***, 2009,** 25, 2667. (b) Rakap, M., Özkar, S., *Applied Catalysis B: Environmental*,**2009**, 91, 21.

[35] (a) Rakap, M., Özkar, S., *Int. J. Hydrogen Energy,* **2010,** 35, 3341. (b) Rakap, M., Özkar, S., *Int. J. Hydrogen Energy,* **2010**,35, 1305.

[36] (a) Mori, K., Hara, T., Mizugaki, T., Ebitani, K., Kaneda, K., *J. Am. Chem. Soc.*, **2004**, 126, 10657.(b) Ho, C. M., Yu, W. Y., Che, C.-M., *Angew. Chem., Int. Ed.*, **2004**, 43, 3303. (c) Mitsudome, T., Arita, S., Mori, H., Mizugaki, T., Jitsukawa,

K., Kaneda, K., *Angew. Chem., Int. Ed.*, **2008**, 47, 7398. (d) Liu, Y., Tsunoyama, H., Akita, T., Tsukuda, T., *Chem. Commun*., **2010,** 46, 550.

[37] (a) Zahmakıran, M., Tonbul, Y., Özkar, S., *Chem. Commun.*,**2010**, 46, 4788. (b) Rakap, M., Özkar, S., *Int. J. Hydrogen Energy*, **2011**, 36, 7019. (c) Rakap, M., Özkar, S., *Catalysis Today*, 2011, doi:10.1016/j.cattod.2011.04.022.

[38] Kaneda, K., Mizugaki, T., *Energy Environ. Sci.*, **2009**, 2, 655.

[39] Astruc, D., Lu, F., Aranzaes, J. R. *Angew. Chem., Int. Ed.*, **2005**, 44, 7852.

[40] Annemieke, W.C., Arean, C.O., *Chem. Commun*., **2008**, 668.

[41] Midilli, A., *Renew. Sustain. Energy Rev*., **2005**, 9, 255.

[42]Hydrogen as Alternative Fuel http://www.eere.energy.gov/afdc/fuels/hydrogen_alternative.html, 27/01/2012, (b) Ewan, B.C.R., Allen, R.W.K., Int. J. Hydrogen Energy, **2005**, 30, 809.

[43] Balat, M., *Energy Sources Part A*, **2005**, 27, 569.

[44] Sherif, S.A., Barbir, F., Veziroglu, T.N., *The Electricity Journal*, **2005** Elsevier Inc. doi:/10.1016/j.tej.2005.06.003

[45] Crabtree, G.W., Mildred, S., Dressedhaus, Buchanan, M.V., *Physics Today*, **2004**, 57, 39

[46] Funk, J., *Int. J. Hydrogen Energy*, **2001**, 26, 185.

[47] Levchenko, A., Dobrovolsky, Y., Bukun, N., Leonova, L., Zyubina, T., Neudachina, V., et al. *Russ. J. Electrochem*., **2007**, 43, 552.

[48] Amao, Y., Tomonou, Y., Okura, I., *Sol. Energy Mater. Sol. Cells*, **2003**, 79, 103.

[49] Uhrig, R.E., Capehart, B.L., editor. *Encyclopedia of energy engineering and technology*. Taylor & Francis Group; September 28, **2007**.

[50] Eyma, Y., Alfonso, M., Beaird, A.M., Davis, T.A., Matthews, M.A., *Ind. Eng. Chem. Res.*, **2009**, 48, 3703.

[51] Weast, R.C. *Handbook of chemistry and physics,* 57th edn. CRC, Boca Raton. **1976**.

[52] Russell, H., Thomas, J., Thomas, G., *J. Matter. Sci.*, **2008**, 43, 5395.

[53] Schlapbach, L., Zuttel, A., *Nature*, **2001**, 414, 353.

[54] Züttel, A., *Mater. Today*, **2003**, 6, 24

[55] (a) Schlesinger, H.I., Brown, H.C., Finholt, A.E., Gilbreath, J.R., Hoekstra, H.R., Hyde, E.K., *J. Am. Chem. Soc.*, **1953**, 75, 215. (b) Hoekstra, H.R., Hyde, E.K., *J. Am. Chem. Soc*., **1953**, 75, 215.

[56] Amendola, S.C., Onnerud, P., Kelly, M.T.,, Petillo, P.J., Sharp- Goldman, S.L., Binder, M., *J. Power Sources*, **1999**, 84, 130.

[57] Amendola, S.C., Sharp-Goldman, S.L., Janjua, M.S., Spencer, N.C., Kelly, M.T., Petillo, P.J., Binder, M., *Int. J. Hydrogen Energy*, **2000**, 25, 969

[58] (a) Demirci, U.B., Miele, P., *C. R. Chim*., **2009**, 12, 943. (b) Demirci, U. B., *J. Power Sources*, **2007**, 172, 676. (c) Liu, B. H., Li, Z.P., *J. Power Sources*, **2008**, 187, 527.

[59] U.S. Department of Energy. Independent review.. Go/no-go recommendation for sodium borohydride for on-board vehicular hydrogen storage. November **2007.**

[60] (a) Langmi, H.W., McGrady, G.S., *Coord. Chem. Rev.*, **2007**, 251, 925. (b) Hamilton, C.W., Baker, R.T., Staubitz, A., Manners, I., *Chem. Soc. Rev*., **2009**, 38, 279. (c) Gutowska, A., Li, L., Shin, Y., Wang, C.M., Li, X.S., Linehan, J.C., Smith, R.S., Kay, B.D., Schmid, B., Shaw, W., Gutowski, M., Autrey, T., *Angew. Chem. Int. Ed.*, **2005,** 44, 3578.

[61] (a) Custelcean, R., Dreger, Z. A., *J. Phys. Chem. B*, **2003,** 107, 9231. (b) Horvath, V., Kovacs A., Hargittai, I., *J. Phys. Chem. A*, **2003**, 107 1197.

[62] Staubitz, A., Robertson, A.P.M., Sloan, M.E., Manners, I. *Chem. Rev*. **2010**, 110, 4023.

[63] Klooster, W.T., Koetzle, T.F., Siegbahn, P.E.M., Richardson, T.B., Crabtree, R.H., *J. Am. Chem. Soc.*, **1999**, 121, 6337.

[64] Hugle, T., Kuhnel, M. F., Lentz, D., *J. Am. Chem. Soc*., **2009**, 131, 7444.

[65] (a) Karahan, S., Zahmakıran, M., Özkar, S., *Int. J. Hydrogen Energy*, **2011**, 36, 4958. (b) Çelik, D., Karahan, S., Zahmakıran, M., Özkar, S., *Int. J. Hydrogen Energy*, **2012**, doi:10.1016/j.ijhydene.2011.12.067.

[66]Schmid, G., Bäumle, M., Geerkens, M., Heim, I., Osemann, C., Sawitowski, T., *Chem. Soc. Rev.*, **1999**, 28, 179.

[67] Aiken III, J.D., Lin, Y., Finke, R.G., *J. Mol. Catal. A: Chem.*, **1996**,114, 29.

[68] Feldheim, D. R., Foss Jr, C. A. (Eds.), *Metal Nanoparticles: Synthesis, Characterization, and Applications*, Marcel Dekker, NewYork, **2002**.

[69] (a) Schmid G., Ed.., *Clusters and Colloids: From Theory to Applications*, VCH Publishers, New York, **1994**. (b) De Jongh, L.J.,_Ed.., *Physics and Chemistry of Metal Cluster Compounds*, Kluwer Publishers, Dordrecht, **1994.**

[70] Simon, U., Schön, G., Schmid, G., *Angew Chem. Int. Ed. Eng*., **1990**, 248, 1186.

[71] Glanz, J., *Science*, **1995**, 269, 1363.

[72] Antonietti, M., Göltner, C., *Angew Chem. Int. Ed. Eng.*, **1997**, 36, 910.

[73] Elghanian, R., Storhoff, J.J., Mucic, R.C. Setinger, R.L. Mirkin, C.A.; *Science*, **1997**, 277, 1078.

[74] Colvin, V.L., Schlamp, M.C., Alivisatos, A.P., *Nature*, **1994**, 370, 354.

[75] Vossmeyer, T., Delenno, E., Heath, J.R., *Angew. Chem., Int. Ed. Eng*., **1997**, 36, 1080.

[76] (a) Schmid, G., Maihack, V., Lantermann, F., Pechel, S., *J. Chem. Soc. Dalton Trans.*, **1996**, 199, 589. (b) Lin, Y., Finke, R. G., *J. Am. Chem. Soc.*, **1994**, 116, 8335. (c) Bönneman, H.; Braun, G.A., *Angew Chem. Int. Ed. Eng*., **1996**, 35, 1992. (d) Lewis, L.N.; Lewis, N., *J. Am. Chem. Soc.*, **1986**, 108, 7228. (e) Wilcoxon, J.P.; Martinho, T.; Klavetter, E.; Sylwester, A.P., *Nanophase Mater*. **1994**, 771. (f) Na, Y.; Park, S.; Bong, S.H.; *J. Am. Chem. Soc.*, **2004**, 126, 250. (g) Pelzer, K.; Vidoni, O.; Phillot, K.; Chaudret, B.; Colliére, V., *Adv. Func. Mater*., **2003**, 12, 118. (h) Hostetler, M.; Wingate, J.; Zong, C.; Evans, N.; Murray, R., *Langmuir*, **1998**, 14, 17-30 (i) Pelzer, K.; Phillot, K.; Chaudret, B., *Z. Anorg. Allg. Chem.*, **2003,** 629, 1217.

[77] Pool R., Science, **1990,** 248, 1186

[78]Schmid, G., *Endeavour*, **1990**, 14, 172.

[79] Corain, B., Schmid, G., Toshima, N., *Metal Nanoclusters in Catalysis and Materials Science*, Elsevier, Amsterdam, Netherlands, **2008**.

[80] Evans, D. F.; Wennerström, H. *In The Colloidal Domain*, 2nd, ed.; Wiley-VCH: New York, **1999**.

[81] R.J. Hunter, *Foundations of Colloid Science*, Vol. 1, Oxford Univ. Press, New York, **1987**.

[82] A.J. Bard, L.R. Faulkner, *Electrochemical Methods*, Wiley, New York, **1980**.

[83] Ninham, B. W., *Adv. Coll. Int. Sci*., **1999**, 83.

[84] Cao, G., *Nanostructures & nanomaterials: Synthesis, properties and applications*, Imperial College Press, London, **2004**.

[85] Grubbs, R. B., *Polymer Reviews*, **2007**, 47, 197.

[86] Hornyak, G.L., Tibbals, H.F., Dutta, J., Moore, J.J., *Introduction to Nanoscience and Nanotechnology*, CRC Press, New York, **2009**.

[87] Willner, I., Mandler, D., *J. Am. Chem. Soc.*, **1989**, 111, 1330

[88] Bönneman, H., Richards, R. M., *Eur. J. Inorg. Chem.*, **2001**, 10, 2445

[89] (a) Tano, T., Esumi, K., Meguro K., *J. Colloid Interface Sci.*, **1989**, 133, 530. (b) Esumi, K., Tano, T., Meguro, K., *Langmuir*, **1989**, 5, 268. (c) Dhas, N. A., Suslick, K. S., *J. Am. Chem. Soc*., **2005**, 127, 2368. (d) Suslick, K A., Choe, S.-B., Cichowias, A. A., Grinstaff, M. W., *Nature*, **1991**, 353, 414.

[90] Duteil, A., Queau, R., Chaudret, B., Mazel, R., Roucau, C., Bradley, J. S., *Chem. Mater*., **1993**, 5, 341

[91] Klabunde, K. J., Habdas, J., Cardenas-Trivino, G., *Chem. Mater*., **1989**, 1, 481.

[92] (a) Reetz, M. T., Helbig, W., Quaiser, S. A., *In Active Metals:Preparation, Characterization, Applications*, VCH: New York, **1996**. (b) Reetz, M. T., Helbig, W., *J. Am. Chem. Soc.*, **1994**, 116, 7401.

[93] George, S. M., *Chem. Rev*., **2010**, 110, 111.

[94] Martinez, A., Prieto, G., *Catal. Commun*., **2007**, 8, 1479.

[95] (a) Cui, H., Zayat, M., Levy, D., *Chem. Mater*., **2005**, 17, 5562. (b) Wang, C.-C., Ying, J. Y., *Chem. Mater.*, **1999,** 11, 3113.

[96] Farrauto, R. J., Bartholomev, C. H., *Fundamentals of Industrial Catalytic Processes*, John Wiley and Sons, New York, **2005**.

[97] Catalysis Principles, http://www.catalysis-ed.org.uk/principles/mechanism.htm, 27/01/2012.

[98] Emig, G., Chemie in unserer Zeit**. 1987**, 21, 128.

[99] (a) Rothenberg, G. *Catalysis: Concenpts and Green Applications*, Wiley-VCH, Weinheim, **2008**. (b) Smith, G.V., Notheisz, F., *Heterogeneous Catalysis in Organic Chemistry*; Academic Press, San Diego, **1999**. Gunderloy, F.C., Hydrazine -mono- and bisborane, McGraw-Hill Book Company, Inc; 1967, p. 13-16.

[100] Hagen, J., *Industrial Catalysis*, Wiley-VCH, Weinheim, **2006.**

[101] Williams, D.B., Carter, C.B., Transmission Electron Microscopy, A Textbook for Materials Science, Plenum, New York, **1996**.

[102] (a) Metin, Ö.; Özkar, S. *Int. J. Hydrogen Energy*, **2007**, 32, 1707. (b) Metin, Ö.; Özkar, S. *J. Mol. Catal. A: Chem.*, **2008**, 295, 39. (c) Metin, Ö.; Özkar, S. *Energy&Fuels*, **2009**, 23, 3517. (d) Erdogan, H.; Metin, Ö.; Özkar, S. *Phys. Chem. Chem. Phys.*, **2009,** 11, 10519. (e) Metin, Ö.; Sahin, S.; Özkar, S. *Int. J. Hydrogen Energy*, **2009,** 34, 6304.

[103] Gunderloy, F. C., *Hydrazine- mono- and Bisborane*, McGraw- Hill Book Company, Inc, **1967**.

[104] Breck DW. *Zeolite molecular sieves*. New York: Wiley; **1974.**

[105] Jones, I. P., *Chemical microanalysis using electron beams*, The Institute of Materials, London, **1992**.

[106] Kaneko, K., *Journal of Membrane Science*, **1994**,96, 59.

[107] Mevellec, V., Nowicki, A., Roucoux, A., Dujardin, C., Granger, P., Payen, E., et al. *New J. Chem.*, **2006**, 30, 1214.

[108] (a) Selvam, P., Viswanathan, B., Srinivasan, V., *J. Electron Spectrosc. Relat. Phemon.*, **1989**, 49, 203. (b) Sugama, T., KuKacka, L.E., Carciello, N., Hocker, N.J., *Cement and Concrete Research*, **1989**, 19, 857.

[109] Landis, W.J., Martin, J.R., *J. Vac. Sci. Technol. A*, **1984**, 2, 1108.

[110] Laidler ,K.J., *Chemical Kinetics*, Benjamin-Cummings UK, 3rd edn., **1997**.

[111] Eyring, H., *J. Chem. Phys.*, **1935**, 3, 107.

[112] Guella, G., Zanchetta, C., Patton, B., Miotello, A., *J. Phy. Chem. B*, **2006**, 110, 17024.

[113] Xu, Q., Chandra, M., *J. Power Sources*, **2006**, 163, 364.